Structural Basis for the Functional Dynamics of the SufBCD Complex Involved in *de Novo* Fe-S Cluster Biogenesis

（ダイナミックな構造変化が駆動する鉄硫黄クラスター生合成機構の構造基盤）

Doctoral thesis

Kei Hirabayashi

2015

Graduate School of Science

Osaka University

Abbreviations

Fe-S	iron-sulfur
E. coli	*Escherichia coli*
ABC	ATP-binding cassette
DTT	dithiothreitol
MIRAS	multiple isomorphous replacement method coupled with anomalous scattering
r.m.s.d.	root mean square deviation
RCT	random conical tilt
EM	electron microscopy
SAXS	small angle X-ray scattering
MVA	mevalonate
MEP	2-*C*-methyl-D-erythritol 4-phosphate
PDB	Protein Data Bank
TMD	transmembrane domain
SMC	structural maintenance of chromosome
ANS	1-anilinonaphthalene-8-sulfonate
DACM	*N*-(7-dimethylamino-4-methylcoumarinyl)-maleimide

Contents

General Introduction

Properties and functions of Fe-S cluster

Iron-sulfur (Fe-S) clusters were identified about 50 years ago as acid-labile prosthetic groups contained within a class of electron carrier proteins called ferredoxins (1). The role of Fe-S clusters as agents of electron transfer is ideally suited to their versatile electronic properties (2). This feature remained the only known function of Fe-S clusters until nearly 20 years later, when it was discovered that aconitase, a key player in the TCA cycle, also contains an Fe-S cluster (3). Aconitase does not have a redox function but rather catalyzes the reversible isomerization between citrate and aconitate, in which Fe-S cluster is responsible for this reaction. In more recent years, over 100 different proteins that contain Fe-S clusters, generically called Fe-S proteins, have been found and the functional diversity of their associated clusters is remarkable (4). As examples, Fe-S clusters are now known to have roles in controlling protein structure, to act as environmental sensors, to serve as modulators of gene regulation, and to participate in radical generation. Such functional diversity almost certainly reflects the chemical versatility of iron and sulfur (2).

The most typical Fe-S clusters have the forms of [2Fe-2S], [3Fe-4S], and [4Fe-4S] and these are usually coordinated to their cognate proteins by the thiolate side chains of cysteine residues (Fig. G-1). However, not all Fe-S clusters are uniquely attached to their protein partners by cysteine ligands; occasionally coordinated by imidazole nitrogen of the histidine residue, carboxyl oxygen of the aspartic acid residue, hydroxyl oxygen of the serine residue, or backbone amides (5). Also, not all Fe-S proteins contain clusters that have Fe as the only metal; the nitrogenase MoFe protein contains a cluster, called FeMo-cofactor, which has a [7Fe-9S-Mo] core (6). Furthermore, unlike the binding manner of many other prosthetic group types, there is

not a single canonical sequence that defines an Fe-S cluster-binding motif within polypeptides. In fact, variations in the spacing, environment and types of Fe-S cluster ligands found in different Fe-S proteins is a significant contributor to the wide range of the electronic and chemical properties of their associated Fe-S clusters.

It was shown in 1960s that simple [2Fe-2S] and [4Fe-4S] clusters can be removed from polypeptide by chelation and then reconstituted by simply incubating the apo-protein in the presence of $Fe^{2+/3+}$ and S^{2-} under reducing conditions (7). An important observation was that the correct cluster type could be reassembled by this method. It has thus been considered for a long time that, inside the cells, Fe-S clusters may form spontaneously, simply requiring iron and sulfide. However spontaneous, intracellular assembly of Fe-S clusters is not an attractive prospect because these elements are metabolic poisons. Hence it was expected that *in vivo* this process would be facilitated by protein factors in order to avoid the accumulation of $Fe^{2+/3+}$ and S^{2-} to toxic levels.

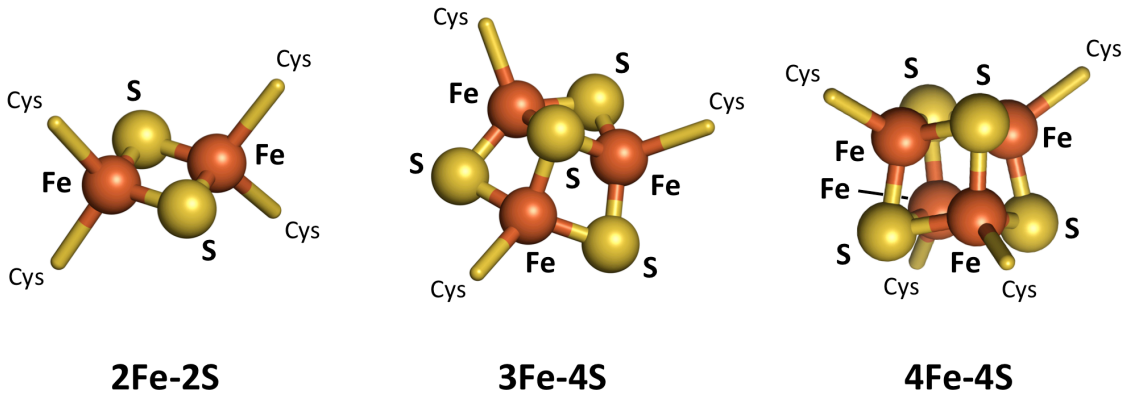

Figure G-1. Typical three types of the Fe-S cluster. The clusters are coordinated in general by thiolate side chains of cysteine residues. Iron and sulfur atoms are colored in red and yellow, respectively.

Systems responsible for Fe-S cluster biogenesis

From the late 1980s to the early 2000s, genetic and biochemical studies revealed three distinct systems that can direct Fe-S protein maturation *in vivo* one after another (8-10). The first system to be discovered was the so-called NIF system (Fig. G-2A) from *Azotobacter vinelandii*, which is required for the activation of the catalytic components of the biological nitrogen fixation, nitrogenase (8). The NIF system includes two proteins, NifS and NifU, which are responsible for the pyridoxal phosphate-dependent mobilization of S using L-cysteine (cysteine desulfurase) and for providing a scaffold for nascent Fe-S cluster assembly, respectively (11-15). More recently, it has been shown that the NIF type of system for Fe-S protein maturation is not necessarily restricted to nitrogen-fixing organisms, because proteins bearing a high degree of similarity to NifS and NifU have been identified in some anaerobic organisms lacking nitrogenase. They appear to be required for the general maturation of Fe-S proteins in those organisms (16-18).

A second, more complicated system for Fe-S protein maturation is referred to as the ISC system (Fig. G-2B), which includes eight contiguously arranged genes encoding IscR, IscS, IscU, IscA, HscB, HscA, Fdx, and IscX in several bacteria (9,19,20). For simplicity, this genomic region is generically referred to as the "*isc*" gene region. IscS and IscU bear primary sequence similarity and have functions analogous to NifS and NifU respectively, in which IscU corresponds to the N-terminal domain of NifU. IscA has been proposed to serve as either an alternative scaffold or an agent of iron delivery to the IscU scaffold (21-24). HscA and HscB bear primary sequence similarity to Hsp70 chaperone DnaK and its cognate cochaperone DnaJ, respectively, and have therefore been proposed to have a chaperone function related to Fe-S protein maturation. Fdx carries a stable, redox-active [2Fe-2S] cluster itself, and is involved presumably in the reduction step of sulfur and/or iron atoms. IscX is a small acidic protein sharing several features with frataxin/CyaY, and likely serves as iron chaperone. IscR is a

regulatory protein that apparently controls the expression of the *isc* gene cluster in a negative feedback loop that involves the assembly of a [2Fe-2S] cluster within IscR (25). The components of the ISC machinery are conserved in α-, β-, and γ-proteobacteria and also in mitochondria from lower to higher eukaryotes (18).

A third system for Fe-S protein maturation, discovered in *Escherichia coli*, is called the SUF system (10) (Fig. G-2C). In *E. coli*, the SUF system is comprised of SufA, SufB, SufC, SufD, SufS, and SufE, and it functions under conditions of oxidative stress or Fe limitation, when the ISC system is apparently inadequate (26,27). SufS and SufE represent a two-component cysteine desulfurase with a function that is analogous to those of NifS and IscS (28,29). SufA bears primary sequence homology to IscA and has been proposed to serve as either an iron donor for the assembly or as a carrier protein transferring Fe-S clusters from a scaffold to target apo-proteins (30-32). The remaining proteins, SufB, SufC, and SufD, have attracted much attention because deletion of any of them abolishes SUF function *in vivo* (10,18,27). These three components have been shown to form a stable ternary complex (SufBCD), and recent *in vitro* reconstitution studies have suggested that this complex can serve as the scaffold for the nascent Fe-S cluster assembly (29,33-35). The SUF homologs are distributed in plastids as well as in Eubacteria and Archaea (18).

The three biosynthetic systems were being elucidated by genetic and biochemical studies together with their distinct properties as well as interchangeability among the three systems: they all are responsible for maturation of a wide variety of Fe-S proteins without strict specificity for apo-protein targets or Fe-S cluster types (either [2Fe-2S], [3Fe-4S], or [4Fe-4S]) to be assembled. The central concept is that the three biosynthetic systems share mechanistic similarity in the requirement for a cysteine desulfurase (sulfur donor) and the participation of an Fe-S scaffolding protein for assembly of a nascent, labile Fe-S cluster prior to delivery to the

target apo-proteins. Hence, the biosynthetic reactions are postulated as follows (Fig. G-2): First, the sulfur atom is abstracted from the substrate cysteine by the action of cysteine desulfurase NifS/IscS/SufS to produce alanine and enzyme-bound sulfane sulfur (S^0). Second, the sulfur atom is transferred to the scaffold protein NifU/IscU/SufBCD by specific protein-protein interaction between the scaffold protein and the cognate cysteine desulfurase. Third, upon supply of iron atoms and reducing equivalents (by an as yet unknown mechanism), a transient Fe-S cluster is assembled on the scaffold. Finally, the pre-assembled cluster is delivered to recipient apo-proteins to form the active site of Fe-S proteins. However, important mechanistic questions have remained to be solved; How Fe-S clusters are assembled on the scaffold protein? How various accessory components participate in Fe-S cluster biosynthesis? How they interact and cooperate with other components? Given the importance of Fe-S proteins to so many cellular processes, the Fe-S cluster biosynthesis is an exciting area of research with many open questions.

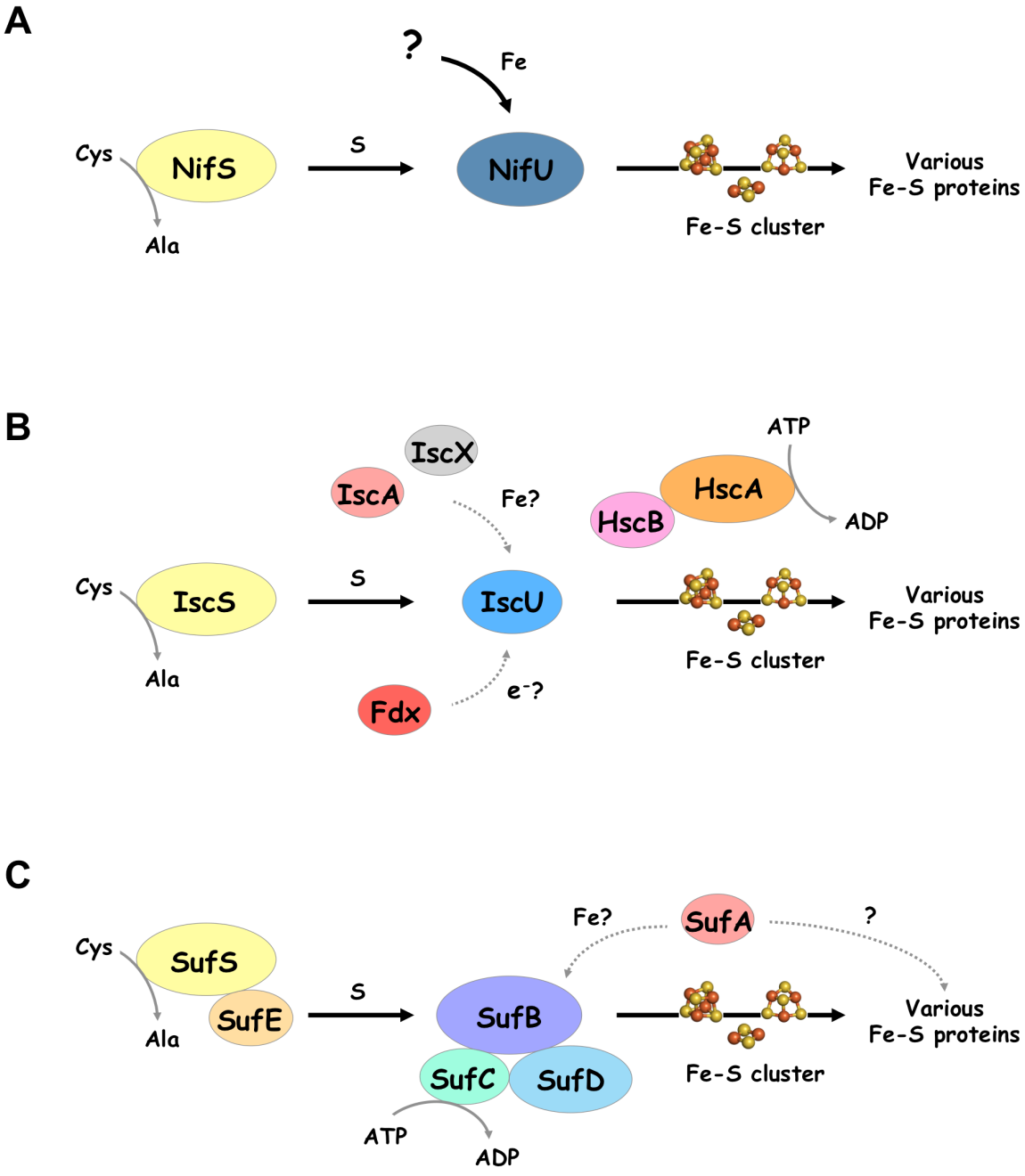

Figure G-2. Comparison of the three systems responsible for Fe-S cluster biogenesis. The three systems are composed of cysteine desulfurase (NifS/IscS/SufS) and other components that act in concert in the assembly of intermediate Fe-S cluster and the subsequent transfer of these clusters to target proteins. (A) NIF machinery. (B) ISC machinery. (C) SUF machinery.

Recent advances in the studies of the SUF pathway

The SUF system is the most ancient/widespread among the currently identified Fe–S cluster biogenesis systems (10). The widespread taxonomic distribution of SUF and its presence in both aerobes and anaerobes suggest this system evolved prior to the widespread oxygenation of the biosphere (36). The *suf* operon is diverse and can contain from two to more than six genes organized as (presumed) single polycistronic transcriptional units. The simplest *suf* operon that contains the minimal functional core is comprised solely of *sufBC* (10), which system is widely distributed in many Archaea. Thus, the ancestral *suf* operon likely consisted of only *sufBC*. A number of organisms contain the *sufBC* genes and lack *sufD*; however, there is currently no evidence of *sufCD* being found in the absence of *sufB* in any genome. This finding coupled with the substantial sequence homology between SufB and SufD suggests that *sufD* results from a duplication of *sufB* (36).

The SUF machinery has been the focus of intense studies at the biochemical level, especially in *E. coli*. As described above, the *sufABCDSE* operon in *E. coli* encodes six proteins. SufS and SufE interact in a complex (SufS-SufE) (28). The cysteine desulfurase SufS mobilizes sulfur from free cysteine, resulting in formation of a persulfide on SufS Cys364 (37). The persulfide sulfur atom is then donated from SufS to the active-site Cys51 on the SufE protein (29,38). Consequently, the presence of the SufE sulfur transfer shuttle stimulates the basal activity of SufS, and the two proteins together form a novel sulfur transfer system (28,29).

The function of SufA was more enigmatic. Some *in vitro* experiments had shown that SufA can bind ferric iron and transfer it to IscU during cluster assembly (31). However, recent *in vitro* experiments unambiguously demonstrated that SufA binds a [2Fe-2S] cluster that can be transferred to target apo-proteins (32). Consequently, SufA could be defined either as an iron donor for the Fe-S cluster assembly or as a carrier protein transferring Fe-S clusters from a

scaffold to a target protein. Genetic studies supported the latter concept, and SufA was included in the family of the so-called A-type carriers (39).

The three remaining components of the SUF machinery, SufB, SufC, and SufD, were shown to be essential for *in vivo* Fe-S biosynthesis (10,27,33). SufC is encoded along with SufB in all *suf* operons identified in sequenced genomes. The SufC homologs, which all share at least 30% sequence identity, have strictly conserved Walker A and Walker B motifs that are commonly found in nucleotide triphosphate-binding proteins, and have actually been shown to exhibit ATPase activity (33,40). More interestingly, SufC shares limited sequence similarity ($\leqslant$25% identity) with members of the ATP-binding cassette (ABC) ATPase superfamily (41).

SufB and SufD share similarity in both primary and secondary structures with each other (17% identity and 37% similarity), and interact with SufC to form a tight SufBCD complex (29,33). Although the two other states of subcomplex have been reported: the SufBC subcomplex and the SufCD subcomplex (42-44), their physiological rolls in SUF machinery remain currently unclear. *In vitro* kinetic experiments have reported that SufC ATPase activity is enhanced by interacting with SufD and further as part of the SufBCD complex (43,45). Physical interaction between the SufBCD complex and the SufSE complex results in further stimulation of the cysteine desulfurase activity of the SufSE complex (29,46). SufA was also shown to interact with the SufBCD complex (34). And, recent *in vitro* reconstitution studies have suggested that this complex can serve as the scaffold for the nascent Fe-S cluster assembly (29,33-35). Thus, it seems that the SufBCD complex plays a central role in SUF machinery.

Structural studies of proteins can provide critical insights for understanding the detailed functional mechanism. So far, the crystal structures of SufS, SufE, SufA, SufC, SufD, and the SufCD subcomplex (41,44,47-50) have been determined.

The structure of the SufS cysteine desulfurase exhibits striking similarity with IscS, and reveals that the active-site Cys364 of SufS is oriented into the protein interior and does not appear to be solvent accessible (47,51). In contrast, the active-site Cys of the IscS desulfurase is highly exposed on a flexible loop structure (52). These differences in active-site orientation affect basal enzyme activity, since the specific activity of IscS is 20 times higher than that of SufS when the enzymes are assayed alone (53). However, the addition of the SufE sulfur transfer partner increases SufS activity so that it is comparable to that of IscS (28,29). Interestingly, the active-site Cys51 of SufE is also oriented into the protein interior, as shown by the SufE structure (48). Interactions between SufS and SufE must somehow allow their solvent-inaccessible active-site Cys residues to contact each other to allow sulfur transfer from SufS to SufE.

The crystal structure of SufA has some similarities with that of IscA, except that SufA is dimeric while IscA is tetrameric (49). The SufA dimer interface shows two of the invariant Cys residues (Cys114 and Cys116) from each monomer positioned at the dimer interface in an orientation that could allow coordination of iron or an Fe-S cluster between subunits. Interestingly, the Glu118 residue from each SufA subunit is located near Cys114 and Cys116 in the dimer interface, possibly to provide carboxylate ligands for direct iron binding.

Monomeric SufC exhibits striking structural similarity with ABC ATPases, but curiously, the local conformation of SufC, in particular the ATP binding segments, is unique and distinct from that of most other ABC-ATPase family members. Glu171, an invariant catalytic residue in the Walker B motif of SufC, is rotated away from the ATP binding pocket and forms a salt bridge with Lys152 in a neighboring domain (41,54). This conformation of the active site within the monomeric SufC is unfavorable for ATPase activity and seems to represent an inactive, resting form of SufC that prevents wasteful ATP hydrolysis.

The Structural GenomiX project team has also determined the crystal structure of the SufD homodimer, and demonstrated that SufD has a novel fold in which 20 β-strands are assembled into a right-handed parallel β-helix (50). The physiological roll of SufD in SUF machinery remains enigmatic.

The crystal structure of the SufCD subcomplex exhibits the tetrameric architecture ($SufC_2$–$SufD_2$), where each SufC subunit is bound near each C-terminus of homodimeric SufD (44). Although there is currently no direct structural characterization of the SufBCD complex, it is likely that similar interactions occur between SufC and the SufB or SufD partner protein. This is because SufB and SufD share sequence similarity in particular at the regions involved in intersubunit interactions in the SufCD subcomplex (44). In addition, SufBCD forms a complex with a stoichiometry of approximately 1:2:1 (29). Based on these data, I have assumed that the SufBCD ($SufB_1$-$SufC_2$–$SufD_1$) complex most likely shares a common configuration with the SufCD ($SufC_2$–$SufD_2$) subcomplex where one SufD subunit is replaced by the SufB subunit and SufB interacts with both SufC and SufD.

Despite the progress in elucidating their biochemical properties, including three-dimensional crystal structures, the detailed molecular mechanism for SUF machinery remains unclear. Since the SUF pathway requires a complex network and protein-protein interactions of various proteins, the structural information of the protein complex is essential for the further understanding, especially the core complex of SufBCD.

Focus of this study

The goal of this thesis is to unravel the complex SUF system involved in the assembly of Fe-S clusters by combined structural and biochemical studies. As described above, it is clear that the SufBCD complex plays a central role in SUF machinery as a scaffold, but the molecular mechanism underlying Fe-S cluster biogenesis in the SufBCD complex is unknown. In this study,

I approach the subject from the characteristic SufC component as an important player to reveal the mechanism.

SufC is a member of the ABC ATPase superfamily and exhibits ATPase activity. ABC ATPases are chemo-mechanical engines involved in diverse biological pathways defined as the nucleotide-binding components of ABC proteins, almost all of which are membrane transporters (ABC transporters). Although the ABC protein includes several hundred different proteins and has extreme functional diversity, these proteins share a similar architecture, consisting of two ABC ATPase domains bound to substrate/function-specific partner domains; the ABC ATPase activity drives the conformational changes in partner domains required for each function (55). Therefore, it is no surprise to imagine that the similarity with the ABC ATPase in SufC could be positively correlated with the functional mechanism of the SufBCD complex.

Chapter I describes the crystal structure of the SufBCD ($SufB_1$-$SufC_2$-$SufD_1$) complex, providing the first demonstration of the quaternary configuration of the ternary complex. The structure showed the common configuration with ABC proteins, and the core domain of the SufB and SufD subunits has a novel β-helix structure, which is the structural motif specifying Fe-S cluster biosynthesis. *In vitro* activity measurements and *in vivo* complementation assays with mutated SufC demonstrated that SufC can behave as an ABC-type ATPase, and the activity is indispensable for *in vivo* Fe–S cluster assembly.

In Chapter II, the biochemical experiments based on the static crystal structure demonstrated the dynamic characteristic of the SufBCD complex. The two SufC ABC ATPase subunits form a head-to-tail dimer in the complex upon ATP binding, thereby inducing a structural change in the interface between the SufB and SufD subunits. These findings, together with *in vivo* mutational analyses, provided insights into the mechanism of Fe–S cluster assembly in the SufBCD complex.

Chapter I

Crystal structure of the SufBCD complex that serves as scaffold for Fe-S cluster biogenesis

Abstract

Iron–sulfur (Fe–S) clusters, which serve as cofactors for many essential proteins, execute a large spectrum of biochemical tasks in all kingdoms of life. Intracellular formation of the Fe-S cluster in a large number of eubacteria and archaea, as well as eukaryotic chloroplasts is achieved by the SUF machinery. This machinery is encoded in *Escherichia coli* by the *sufABCDSE* operon, where three SUF components, SufB, SufC, and SufD, form a ternary complex and serve as the biosynthetic apparatus for nascent Fe-S clusters. Here, I determined the first crystal structure of the *E. coli* SufBCD ($SufB_1$-$SufC_2$–$SufD_1$) complex, which exhibits the common architecture of ABC proteins: two ABC ATPase components (SufC) with function-specific components (SufB–SufD protomers). The novel β-helix architecture of the SufB–SufD protomers appears to be specialized for the Fe–S cluster biogenesis systems. Biochemical analyses prove that the residues of the ABC sequence motifs in SufC are responsible for ATPase activity as in the canonical ABC ATPase. Furthermore, complementation assays demonstrate that the ATPase activity of SufC is indispensable for *in vivo* Fe–S cluster assembly. These findings have led me to expect that the SufBCD complex shares a common mechanism of action with ABC proteins despite their distinct functions, in which the activity of ABC ATPase components drives conformational changes of the function-specific components.

Introduction

The SUF machinery has been the focus of intense studies at the biochemical level, especially in *Escherichia coli*. The *sufABCDSE* operon in *E. coli* encodes six proteins. SufS cysteine desulfurase and SufE sulfur shuttle protein together provide sulfur from the substrate cysteine for the construction of nascent Fe–S clusters (28,46). SufA is a member of the A-type protein family that transfers Fe-S clusters to target apo-proteins (32). The remaining proteins, SufB, SufC, and SufD, have attracted much attention because deletion of any of them abolishes SUF function *in vivo* (10,18,27). SufC have strictly conserved Walker A and Walker B motifs that are commonly found in nucleotide triphosphate-binding proteins, and have actually been shown to exhibit ATPase activity (33,40). SufB share similarity in both primary and secondary structures with SufD (17% identity and 37% similarity) and interact with SufC to form a stable ternary SufBCD complex (29,33). *In vitro* kinetic experiments have reported that SufC ATPase activity is enhanced by interacting with SufD and further as part of the SufBCD complex (43). Physical interaction between the SufBCD complex and the SufSE complex results in further stimulation of the cysteine desulfurase activity of the SufSE complex (29,46).

Despite the progress in elucidating some of its biochemical properties, including three-dimensional crystal structures of SufC, SufD, and the SufCD subcomplex (41,44,50), the understanding of the role of the SufBCD complex remains elusive. Recent *in vitro* reconstitution studies have suggested that this complex can serve as the scaffold for the nascent Fe–S cluster assembly (29,33-35). It is clear that the SufBCD complex plays a central role in SUF machinery, but the molecular mechanism underlying Fe-S cluster biogenesis on the SufBCD complex is unknown. Here, I approach the subject from the characteristic SufC component as an important player to reveal the mechanism.

Intriguingly, SufC shares limited sequence similarity (≲25% identity) with members of the ATP-binding cassette (ABC) ATPase superfamily (41). ABC ATPases are

chemo-mechanical engines involved in diverse biological pathways defined as the nucleotide-binding components of ABC proteins, almost all of which are membrane transporters (ABC transporters). Although the ABC protein includes several hundred different proteins and has extreme functional diversity, these proteins share a similar architecture, consisting of two ABC ATPase domains bound to substrate/function-specific partner domains; the ABC ATPase activity drives the conformational changes in partner domains required for each function (55). Therefore, it is no surprise to imagine that the similarity of SufC with the ABC ATPase could be positively correlated with the functional mechanism of the SufBCD complex.

In this study, I determined the crystal structure of the SufBCD ($SufB_1$-$SufC_2$-$SufD_1$) complex, providing the first demonstration of the quaternary configuration of the ternary complex. The structure showed the common configuration with ABC proteins, and the core domain of the SufB and SufD subunits has a novel β-helix structure, which is the structural motif specifying Fe-S cluster biosynthesis. *In vitro* activity measurements and *in vivo* complementation assays with mutated SufC demonstrated that SufC can behave as an ABC-type ATPase, and the activity is indispensable for *in vivo* Fe–S cluster assembly.

Experimental procedures

Expression and purification of E. coli SufBCD complex

To purify the SufBCD complex, the entire *suf* operon was expressed simultaneously. The plasmid pGSO164, containing the entire *suf* operon under the control of an arabinose-inducible promoter (29), was used to over-express SufABCDSE in the TOP10 strain of *E. coli*. The cells were grown in TB medium containing ampicillin (50 μg/ml) at 37°C. L-arabinose was added to 0.2% (w/v) final concentration when the cultures reached an A_{600} of 0.4–0.6. After 3 hours of SufABCDSE expression at 37°C, the cells were harvested by centrifugation, and the cell pellets were frozen at -80°C. Cell pellets were lysed by sonication in 50 mM Tris-HCl (pH 7.8), 100 mM NaCl, and 1 mM DTT. The soluble fraction was subjected to ammonium sulfate fractionation at 20% saturation. After centrifugation, the supernatant fraction was loaded onto a HiPrep Phenyl FF (low sub) 16/10 column (GE Healthcare), and the bound protein was eluted with a decreasing linear gradient of 20–0% ammonium sulfate. Fractions containing the SufBCD complex were pooled, dialyzed overnight in 50 mM Tris-HCl (pH 7.8) and 1 mM DTT, and then loaded onto a Mono Q HR 5/50 GL column (GE Healthcare) and eluted with a linear gradient of 0–1 M NaCl. The SufBCD complex was further purified by gel filtration using a HiPrep 16/60 Sephacryl S-200 HR column (GE Healthcare) in 50 mM Tris-HCl (pH 7.8) and 150 mM NaCl. Purified SufBCD complex was concentrated and stored at -80°C.

Site-directed mutagenesis was performed using the pGSO164 plasmid as a template and the primers listed in Table I-1. Genes were expressed in mutant cells (YT2512) in which the entire *sufABCDSE* operon was deleted from the chromosome (10), and mutant SufBCD complexes were purified as described for the wild-type complex.

Table I-1. Oligonucleotides used in this study

Oligonucleotide	Sequence	Restriction sites
SufAF	5'-CCGGCTCGAGGTAAATCGATGGACATGC-3'	*Xho*I
SufB-RSc3	5'-CTCCAGAGCTCCACTTAACATGTTTATTCCTTATCCGAC-3'	*Sac*I
SufD-FSc5	5'-CCGGAGCTCTTGACAGATTACGTTCATGTGCTATATC-3'	*Sac*I
SufER	5'-CCGGGCTAGCCAACCGGATGAAAGCTGT-3'	*Nhe*I
SufC-K40R-F	5'-GGGGCCAAACGGTTCGGGCCGTAGTACCTTATCGGCAACG-3'	
SufC-K40R-R	5'-CGTTGCCGATAAGGTACTACGGCCCGAACCGTTTGGCCCC-3'	
SufC-E171Q-F	5'-CCGGAGTTATGCATTCTTGATCAGTCGGACTCCGGGC-3'	
SufC-E171Q-R	5'-GCCCGGAGTCCGACTGATCAAGAATGCATAACTCCGG-3'	
SufC-H203A-F	5'-CGCTCATTCATCATTGTTACGGCCTACCAACGCATTCTCG-3'	
SufC-H203A-R	5'-CGAGAATGCGTTGGTAGGCCGTAACAATGATGAATGAGCG-3'	
SufC-Y86C-F	5'-ATCTTTATGGCCTTCCAGTGTCCGGTGGAGATTCCAGGTG-3'	
SufC-Y86C-R	5'-CACCTGGAATCTCCACCGGACACTGGAAGGCCATAAAGAT-3'	
SufC-C167A-F	5'-GCCATTCTTGATGAGTCGGACTC-3'	
SufC-C167A-R	5'-TAACTCCGGTTCCAGCACCG-3'	
SufB-C405A-F	5'-GCCGACTCAATGCTGATTGGCG-3'	
SufB-C405A-R	5'-CTGAGTGAAATTGCGCGCAT-3'	
SufD-H360A-F	5'-GATGATGTGAAATGCAGCGCCGGCGCGACGGTG-3'	
SufD-H360A-R	5'-CACCGTCGCGCCGGCGCTGCATTTCACATCATC-3'	
SufD-C358A-F	5'-AAATCTATGCAGATGATGTGAAAGCCAGCCACGGCGCG-3'	
SufD-C358A-R	5'-CGCGCCGTGGCTGGCTTTCACATCATCTGCATAGATTT-3'	

The underlined and shaded bases comprise restriction sites and artificial promoter regions respectively.
The double underlines indicate the altered codons for site-directed mutagenesis.

Crystallization and structure determination

Crystallization was performed by the sitting-drop vapor-diffusion method. Crystals of the SufBCD complex were obtained at 4°C using a reservoir solution containing 31% (v/v) pentaerythritol propoxylate (5/4 PO/OH), 100 mM sodium citrate (pH 5.5) and 200 mM KCl (Fig. I-1A). The protein concentration was 35 mg/ml in 50 mM MES (pH 7.0). Mercury and platinum derivatives were obtained by soaking native crystals for 2 hours in mother liquor containing 1 mM methylmercury(II) acetate, 5 mM methylmercury(II) chloride, or 10 mM potassium tetranitro platinate(II). All crystals were transferred to a cryo-protectant solution containing 5% (v/v) 2-methyl-2,4-pentanediol and flash-cooled by immersion in liquid nitrogen. X-ray diffraction data were collected at beamline BL44XU and BL32XU of SPring-8 (Fig. I-1B) and processed with the HKL2000 package (56). Experimental phases were obtained from mercury- and platinum-derivative crystals by the multiple isomorphous replacement method coupled with anomalous scattering (MIRAS) using AutoSol in PHENIX (57). The model was built manually in COOT (58), and the structure was refined with PHENIX. Secondary structures were assigned using PROMOTIF (59), the geometry of the final model was analyzed using PROCHECK (60), and superposition and r.m.s. deviations of the structures were calculated using LSQMAN (61). All structure figures were prepared using PyMOL (62) or UCSF Chimera (63). X-ray data and refinement statistics are given in Table I-2. Coordinates of the X-ray structure of the SufBCD complex and the Hg-bound SufBCD complex have been deposited in the Protein Data Bank, under accession codes 5AWF and 5AWG.

The crystallographic asymmetric unit contained two SufBCD complexes, termed $Complex_1$ and $Complex_2$. Although the electron density for the SufBCD complex was mostly continuous, the densities for some regions were poorly defined: in $Complex_1$, SufB residues 1–33 and 80–156, SufD residues 1–7 and 422–423, $SufC_{SufB}$ residues 244–248, and $SufC_{SufD}$ residues 236–248; in $Complex_2$, SufB residues 1–35 and 79-157, SufD residues 1–7 and

422–423, $SufC_{SufB}$ residues 244-248, and $SufC_{SufD}$ residues 237-248. Accordingly, these residues were not included in the model.

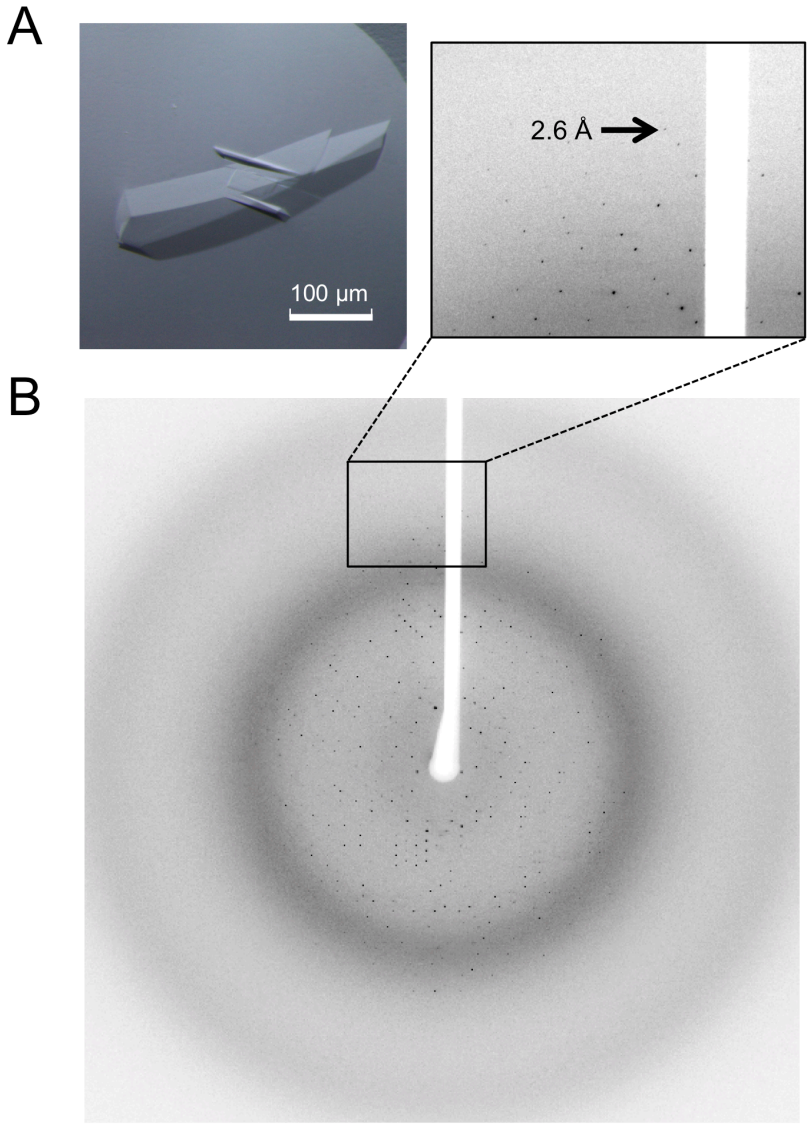

Figure I-1. Crystallographic studies of the *E. coli* SufBCD complex. (A) Crystals of the *E. coli* SufBCD complex. Scale bar indicates 100 µm length. (B) Diffraction pattern of the *E. coli* SufBCD complex crystal. Small panel shows a close up view of the pattern. The resolution of the spot indicated by the arrow is 2.6 Å.

Table I-2. Data collection, phasing and refinement statistics for X-ray crystallography

	Native	Hg derivative 1*	Hg derivative 2†	Pt derivative‡
Data collection				
Space group	$P2_1$	$P2_1$	$P2_1$	$P2_1$
Cell dimensions				
a, *b*, *c* (Å)	119.5, 139.6, 124.7	119.8, 139.4, 124.4	120.2, 140.0, 124.6	119.8, 140.4, 124.5
α, β, γ (°)	90.0, 113.1, 90.0	90.0, 113.6, 90.0	90.0, 113.5, 90.0	90.0, 113.1, 90.0
Resolution (Å)	2.95 (3.06-2.95)	4.30 (4.45-4.30)	4.50 (4.66-4.50)	3.45 (3.57-3.45)
R_{merge} (%)	6.0 (37.1)	12.7 (29.5)	14.4 (29.8)	10.7 (34.1)
$I / \sigma I$	15.8 (2.8)	6.6 (5.2)	5.8 (5.5)	7.6 (4.7)
Completeness (%)	98.5 (98.1)	99.3 (99.9)	92.8 (94.5)	99.1 (99.7)
Redundancy	3.8 (3.6)	5.6 (5.6)	6.0 (5.9)	5.6 (5.6)
Refinement				
Resolution (Å)	41.11-2.95	43.94-4.30		
No. reflections	77,254	50,117		
R_{work} / R_{free} (%)	18.7 / 22.6	29.5 / 34.0		
No. atoms				
Protein	19,914	18,804		
Hg^{2+}	0	4		
B factors (Å^2)				
Protein	83.6	110.3		
Ion	–	148.8		
r.m.s. deviations				
Bond lengths (Å)	0.006	0.007		
Bond angles (°)	1.241	1.672		
Ramachandran plot				
Most favored (%)	92.3	86.5		
Additionally allowed (%)	6.9	12.9		
Generously allowed (%)	0.8	0.6		

*Hg, Methylmercury(II) acetate. †Hg, Methylmercury(II) chloride. ‡Pt, Potassium tetranitro platinate(II).Values in parentheses correspond to the highest-resolution shell.

Single-particle electron microscopy reconstruction

The SufBCD complex was prepared from a peak fraction of gel filtration in 50 mM MES (pH 6.5), 150 mM NaCl, and 5 mM $MgCl_2$. The negatively stained SufBCD complex was examined using an H9500SD transmission electron microscope (Hitachi High-Tech) operated at 200 kV at room temperature. The images were acquired on a 2k × 2k charge-coupled device camera (TVIPS) with a physical pixel size of 0.24 nm. Random conical tilt (RCT) reconstruction was performed using the software package SPIDER (64). The obtained 3D structure from RCT was refined by using the EMAN1 software suite (65). The final reconstruction of the SufBCD complex was computed from ~7,146 particles. The particle images were low-pass filtered at 30 Å before refinement, and therefore the Fourier shell correlation that was calculated using *eotest* of EMAN1 shows higher values than 0.5 in every frequency ranges. The EM structure of the SufBCD complex has been deposited in the Electron Microscopy Data Bank, under accession number EMD-3163.

Solution scattering data collection and analysis

The SufBCD complex (2-18 mg/ml) for small angle X-ray scattering (SAXS) experiments was prepared in 50 mM Tris-HCl (pH 7.8) and 150 mM NaCl. SAXS experiments were performed at room temperature on a Rigaku BioSAXS-1000, using Cu*K*α radiation from the Rigaku FR-X rotating anode X-ray generator. The scattering vector range was set from q_{min} = 0.009 $Å^{-1}$ to q_{max} = 0.69 $Å^{-1}$ ($q = 4\pi\sin\theta/\lambda$). Protein samples were placed in a quartz capillary with a diameter of 1.0 mm using an exposure time of 15 minutes per frame. The final scattering curve was radially averaged from eight frames with the program SAXSLab (Rigaku). Subsequent data was analyzed by the ATSAS program package (66). Data quality was assessed on the basis of the linearity of Guinier plots. Molecular mass was calculated by extrapolating scattering intensity at zero angle, $I(0)$. Scattering profile simulations from the crystal structure

were carried out using CRYSOL (67). *Ab initio* models were generated using DAMMIF (68). 10 individual reconstructions were aligned, averaged and the most typical model was generated using DAMAVER (69). The crystal structure was fitted to the dummy model by manually. The SAXS data at 8 mg/ml measurement were used for Fig. I-4. Data collection and structural parameters are summarized in Table I-3.

Table I-3. Data collection and structural parameters for SAXS analysis

Data Collection Parameters	
Instrument	Rigaku BioSAXS-1000
X-ray source	Rigaku FR-X
Wavelength (Å)	1.54
q range (Å^{-1})	0.009-0.69
Exposure time (min)	15
Concentration range (mg/ml)	2-18
Temperature	Room temperature
Structural Parameters[*]	
$I(0)$ from $P(r)$	0.225 ± 0.001
R_g from $P(r)$ (Å)	40. 8 ± 0.6
$I(0)$ from Guinier	0.222 ± 0.001
R_g from Guinier (Å)	39.9 ± 0.1
Dmax (Å)	138.5
x^2 of DAMMIF models	1.22
Molecular Mass Determination	
M_r from $I(0)$ (kDa)	150.2
M_r from sequence (kDa)	156.7

[*], reported for 8 mg/ml measurement.

In vivo complementation assay with mutated SufC

Site-directed mutations were generated in plasmid pBBR-*sufC* and introduced into *E. coli* mutant strain UT109 (18) harboring two plasmids, pUMV22 and pRK-*sufAB-DSE* (Δ*sufC*p). UT109 contains deletions of the chromosomal *suf* (Δ*sufABCDSE*) and *isc* (Δ*iscUA–hscBA*) operons. Normally, deletion of both pathways is lethal due to the lack of the biosynthetic apparatus for Fe–S clusters (10). However, plasmid pUMV22, which harbors genes for mevalonate kinase, phosphomevalonate kinase, and diphosphomevalonate decarboxylase cloned from *Streptomyces* sp., allows UT109 to grow in the presence of D-mevalonate (MVA) because the essential Fe–S enzymes IspG and IspH involved in the MEP pathway for isoprenoid biosynthesis can be bypassed by the foreign MVA pathway (Takahashi, Y., *submitted for publication*). Upon shift to the absence of MVA, the cells are unable to grow without introduction of a functional *sufC* gene (in this case from pBBR-*sufC*) to complete the partial SUF system provided by pRK-*sufAB-DSE* (Δ*sufC*p).

For the construction of plasmid pRK-*sufAB-DSE* (Δ*sufC*p), the *sufAB* fragment was amplified using primers SufAF and SufB-RSc3, and *sufDSE* was amplified using primers SufD-FSc5 and SufER (Table I-1). Because the coding region of *sufC* contains the promoter elements for *sufDSE*, an artificial promoter sequence was added to the upstream region of *sufD* in the SufD-FSc5 primer. After digestion with restriction enzymes, the two PCR fragments were cloned simultaneously into the *Xho*I/*Nhe*I sites of pRKNSE (19). The expression plasmid pBBR-*sufC* was constructed by transferring the *Xba*I–*Sac*I fragment carrying the ribosome-binding sequence and the SufC coding region from the pET-21a (+) derivative (44) to the pBBR1MCS-4 plasmid (70), in which expression was driven by the *lac* promoter. Mutagenesis of SufC was performed using the pBBR-*sufC* plasmid as a template and the primers listed in Table I-1.

ATP hydrolysis measurement

ATP hydrolysis rates were determined by a linked enzyme assay that coupled the formation of ADP to the oxidation of NADH, as described previously (40).

Protein sequences

The multiple sequence alignments in Figs. I-8 and II-1 were performed using Clustal Omega (71), and the figures were prepared with NJplot (72) and ESPript (73). EcoGene (74) accession numbers for the proteins from *E. coli* K-12 aligned in Figs. I-8 and II-1 are as follows: SufC, EG13964; UgpC, EG11048; MalK, EG10558; PotA, EG10749; PotG, EG11630; ThiQ, EG11572; TauB, EG13299; SsuB, EG12358; ProV, EG10771; GltL, EG12663; YhdZ, EG12837; GlnQ, EG10389; HisP, EG10452; ArtP, EG11624; CysA, EG10183; PstB, EG10783; FetA, EG13259; FepC, EG10295; FecE, EG10290; FhuC, EG10304; BtuD, EG10128; CcmA, EG12059; DppD, EG12627; SapD, EG12304; DdpD, EG13787; DppF, EG12628; UvrA, EG11061; SbcC, EG10927; MutS, EG10625; RecN, EG10831; MukB, EG10618; and RecF, EG10828.

Results

Overall architecture of the SufBCD complex

I determined the first crystal structure of the SufBCD complex from *E. coli* at 2.95 Å resolution (Fig. I-2, A and B) by the multiple isomorphous replacement method coupled with anomalous scattering (MIRAS) phasing from Hg/Pt derivatives. The SufBCD complex consists of one SufB subunit, two SufC subunits, and one SufD subunit with a stoichiometry of 1:2:1, consistent with previous biochemical experiments (44,46). Each of the SufC subunits is bound to a subunit of the SufB–SufD protomers, and is accordingly termed $SufC_{SufB}$ and $SufC_{SufD}$. This overall configuration is common among ABC proteins, in which two ABC ATPase subunits bind to function-specific subunits with their ATP-binding motifs facing each other. The two bound SufC subunits, however, are spatially separated, in contrast to the analogous domains/subunits of canonical ABC transporters; the distance between the SufC subunits within the SufBCD complex is more than 40 Å (Fig. I-2B). Although the asymmetric unit contains two complexes (termed $Complex_1$ and $Complex_2$) with almost identical structures, a slight shift of subunits were observed; two SufC subunits shifted < 1 Å toward each other in the complex. This may implies the mobility of SufC subunits in the complex. The r.m.s. deviation between $Complex_1$ and $Complex_2$ is less than 0.71 Å for the main-chain C_α atoms.

The structure of the SufBCD complex was further examined by 3D-reconstruction imaging based on negative-stain electron microscopy (Fig. I-3). The structures obtained by both methods agreed closely, confirming the quaternary structure of the SufBCD complex. In addition, the crystal structure was consistent with small angle X-ray scattering (SAXS) data from the as-isolated SufBCD complex in solution (Fig. I-4), indicating that the configuration of the SufBCD complex in the crystalline state was not affected by crystal packing.

The structures of SufB and SufD are similar and share a common domain organization: an N-terminal helical domain, a core domain consisting of a right-handed parallel β-helix, and a

C-terminal helical domain that contains the SufC binding site (Fig. I-2A). The β-helix in the core domain of SufB is partly composed of shorter strands than the corresponding domain of SufD, whereas the C-terminal helical domain and the mode of SufC binding are strikingly similar between SufB and SufD. Intriguingly, the mode of binding between the SufC and SufB/SufD subunits is conserved in ABC transporters, an interaction termed the "transmission interface" (75) (discussed below). The heterodimer interface of SufB–SufD protomers consists primarily of 25 hydrogen bonds that form two anti-parallel β-sheets. Although the structure of the SufD subunit in the SufBCD complex was almost identical to that of the previously reported SufD homodimer crystallized alone (50), some structural difference was observed around the two short helix-turn-helix in the C-terminal helical domain (Fig. I-5). This region is located in the interface with SufC, thus it seems that the complex formation induced this structural change. The SufD monomers are superimposable, with an r.m.s. deviation of 0.59 Å between C_α atoms.

The SufC subunit has two domains, as observed in the members of the ABC ATPase family: a catalytic α/β domain that contains the nucleotide-binding Walker A and Walker B motifs, and a helical domain specific to ABC ATPases containing an ABC signature motif (Fig. I-6). The two domains are connected by a Q-loop that contains a strictly conserved glutamine residue. $SufC_{SufB}$ and $SufC_{SufD}$ have almost identical structures (the r.m.s.d. < 0.63 Å), but some minor structural difference was observed in one loop region, which is away from both the catalytic pocket and the binding site with SufB/SufD. This loop region is much more loosely packed in the crystal lattice.

Although the overall structure of SufC subunits in the SufBCD complex is similar to that of monomeric SufC (41), significant structural changes occur around the ATP-binding pocket upon complex formation (Fig. I-7). The unique salt bridge observed in the monomeric SufC between Glu171 (an invariant catalytic residue among typical ABC ATPases (76)) and Lys152 is cleaved in the complex, allowing the rotation of the Glu171 side chain toward the

ATP-binding pocket. Furthermore, His203, another key residue of ABC ATPase activity (77), is shifted about 4 Å toward Glu171 in the complex. These structural changes rearrange the catalytic pocket of SufC to be suitable for ATP binding and hydrolysis; consequently, the local structure of SufC more closely resembles that of active ABC ATPases. Thus, the monomeric SufC is the "latent form" as inadequate for the ATPase activity, whereas SufC in the SufBCD complex appears to represent the "competent form". These findings are consistent with recent kinetic experiments showing that the ATPase activity of SufC is enhanced by complex formation with SufB/SufD (43). Namely, the activity of SufC is regulated with sophisticated structural changes that occur upon binding to its partner proteins.

The SufBCD complex shares a common configuration with the previously reported SufCD subcomplex (44) predictably, in which one SufD subunit is replaced by the SufB subunit, but the physiological roll of SufCD subcomplex in Fe-S cluster biogenesis remains currently unclear (43,44). Although it is possible the SufBCD and SufCD complexes conduct discrete steps in cluster assembly, this has not been conclusively shown *in vivo* or *in vitro*. Because the SufBCD complex is considered to be the biosynthetic apparatus for Fe-S clusters from the pioneering physiological (18,27) and the biochemical (29,34,35) studies, the state of SufCD subcomplex may function by negatively regulating the assembly of Fe-S clusters as the latent form of the SufBCD complex.

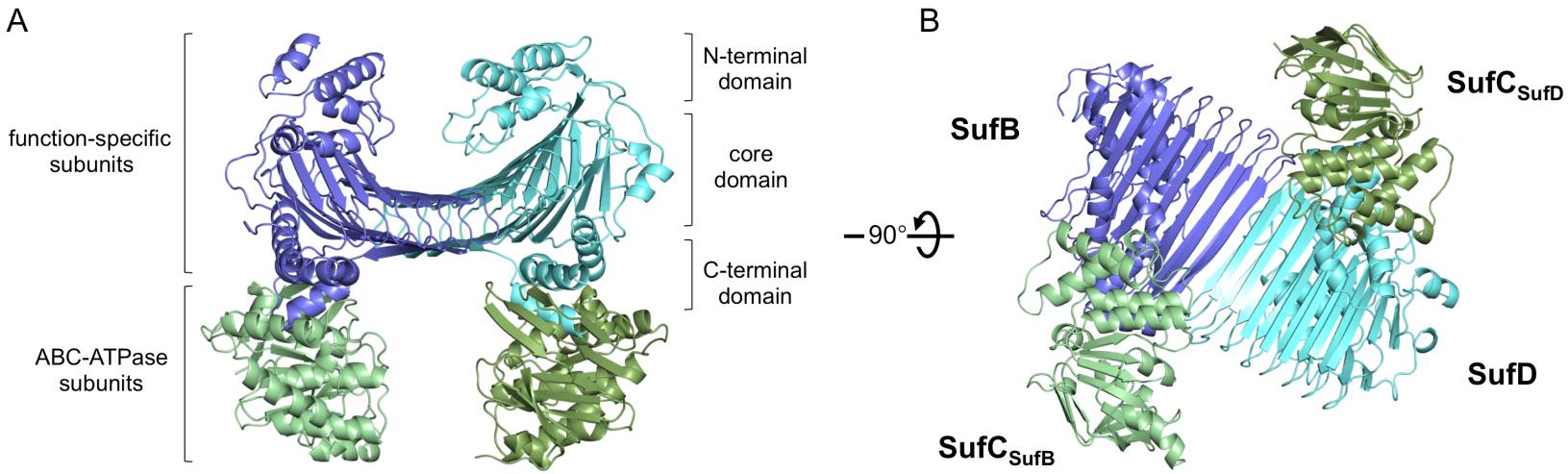

Figure I-2. Overall structure of the SufBCD complex from *E. coli*. (A) Ribbon representation of the crystal structure of the SufBCD complex. Individual subunits are shown in purple (SufB), cyan (SufD), and green (SufC). (B) View rotated by 90º about the horizontal axis relative to (A). Two bound SufC subunits are far from each other compared to other structurally characterized ABC proteins.

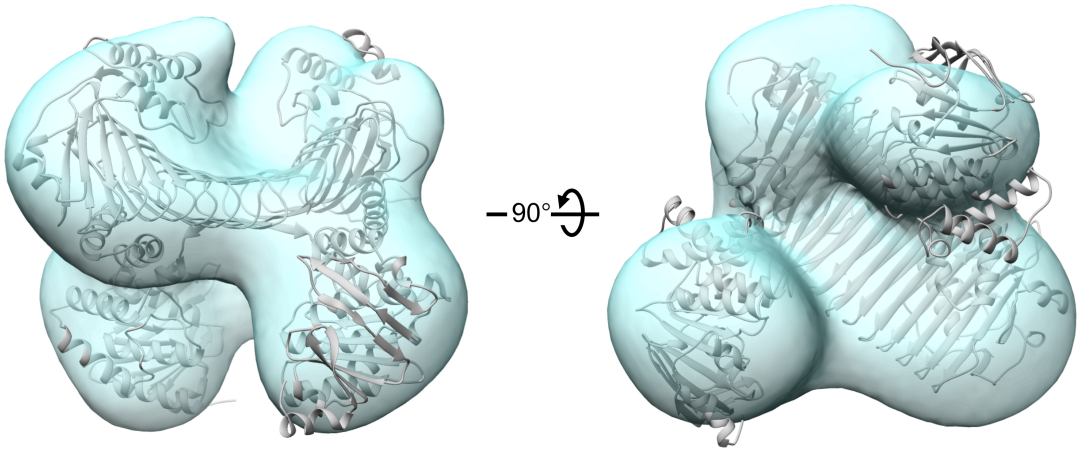

Figure I-3. 3D reconstruction image of the SufBCD complex obtained by electron microscopy. Ribbon representation of the crystal structure of the SufBCD complex (gray) is superimposed on the transparent EM structure (light blue). (right) View rotated by 90º about the horizontal axis relative to (left).

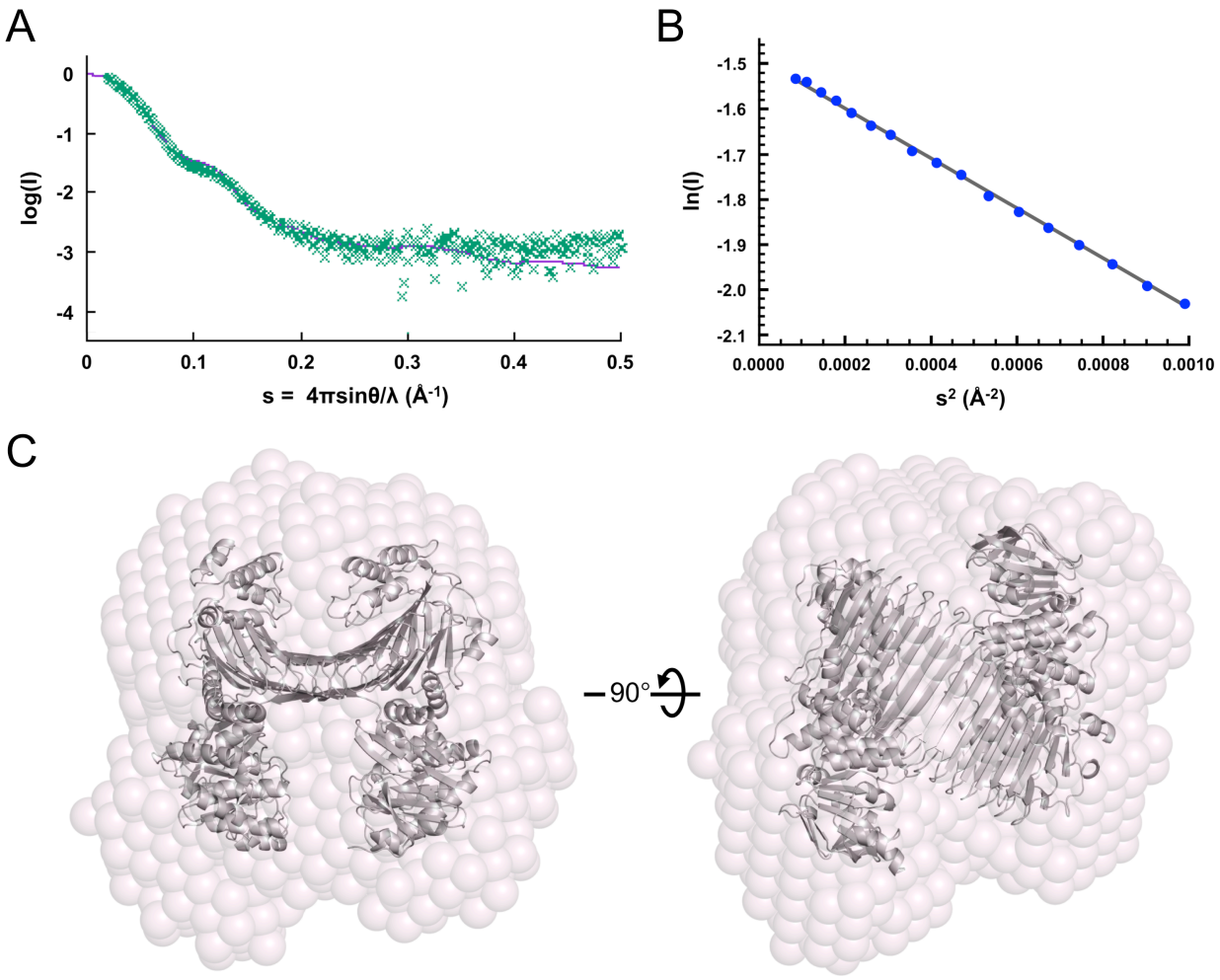

Figure I-4. SAXS analyses of the SufBCD complex. (A) Comparison of the crystal structure and SAXS result. Experimental X-ray scattering curve from the SufBCD complex (green dotted line) and the theoretical curve estimated from the crystal structure (purple solid line). (B) The Guinier plots for the low angle region of the experimental scattering curve at (A). Its linearity indicates the absence of protein aggregation. (C) Molecular modeling of the SufBCD complex in solution. Ribbon representation of the crystal structure of the SufBCD complex (gray) is superimposed on the transparent *ab initio* dummy atom model (pink). (right) View rotated by 90º about the horizontal axis relative to (left).

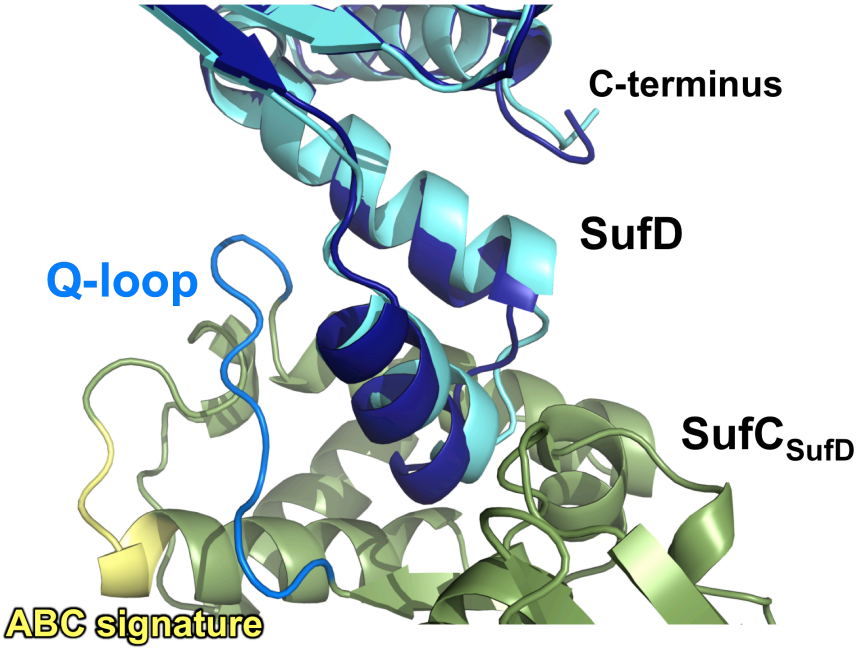

Figure I-5. Local structural difference of SufD upon complex formation with SufC. Close-up view of the interface between SufC subunit (green) and SufD subunit (cyan) in the SufBCD complex. One subunit of the SufD homodimer (PDB code 1VH4, dark blue) is superimposed onto the SufD subunit in the SufBCD complex. Some structural difference was observed around the two short helix-turn-helix located in the interface with SufC. Motifs conserved in ABC ATPases are depicted by different colors: yellow (ABC signature motif) and blue (Q-loop).

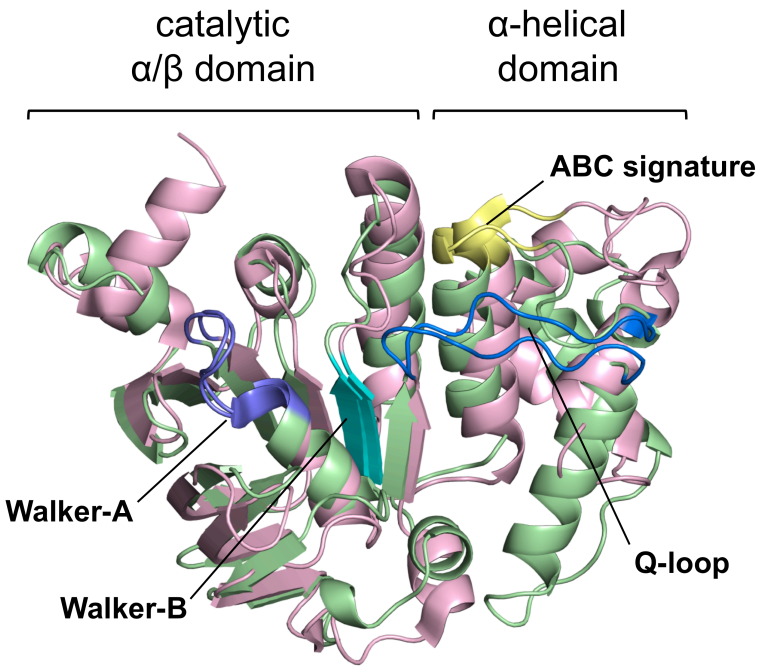

Figure I-6. Superposition of the overall structures of *E. coli* SufC and HlyB (PDB code 1MT0). Green and light pink denote the SufC and HlyB structures, respectively. Motifs conserved in ABC ATPases are depicted by different colors: purple (Walker A motif), cyan (Walker B motif), yellow (ABC signature motif) and blue (Q-loop).

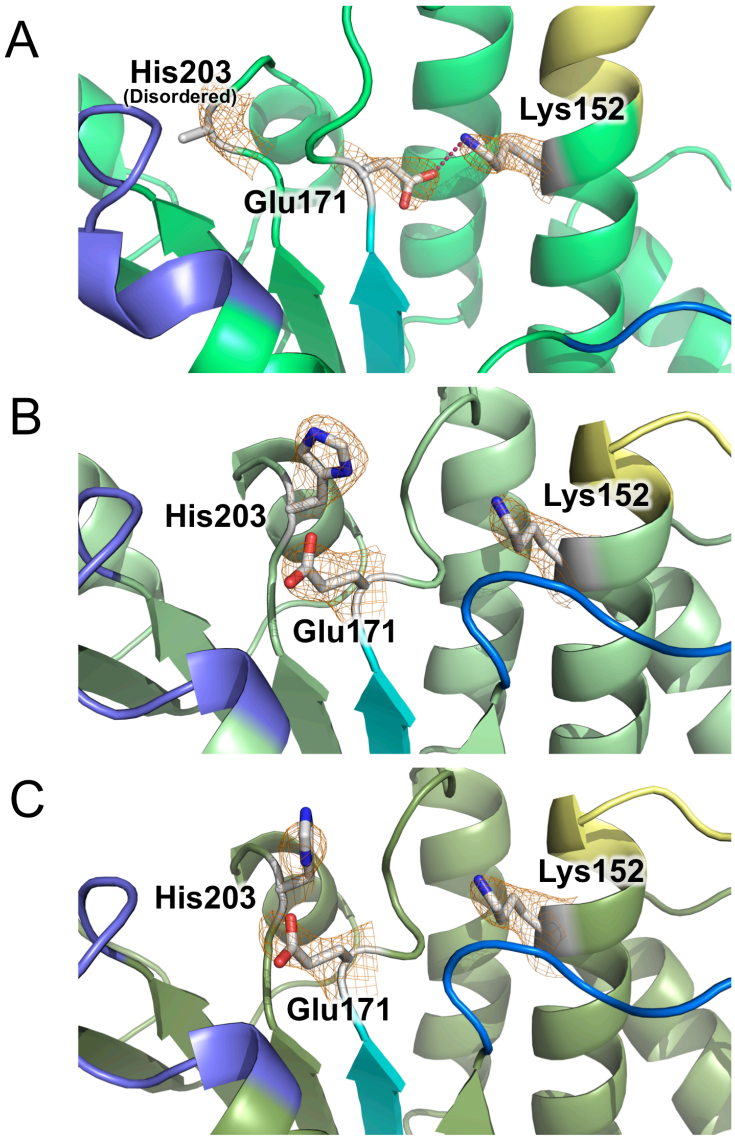

Figure I-7. Structural changes and rearrangements of the ATP-binding pocket in SufC. Comparison of the active site structures of SufC among (A) the SufC monomer (PDB code 2D3W), (B) the $SufC_{SufB}$ subunit, and (C) the $SufC_{SufD}$ subunit. The orientation and color-coding for the conserved motifs in ABC ATPases are the same as in Fig. I-6. Lys152, Glu171, and His203 residues are shown in the stick models, and F_o–F_c maps omitting the side chains of these residues, contoured at 2.0 σ (orange), are overlaid on the stick models. The red broken line in (A) indicates a salt-bridge.

The ABC-type ATPase of SufC

Superposing the structure of *E. coli* SufC on the typical ABC ATPase, *E. coli* HlyB of the α-hemolysin export protein (77), reveals very similar overall topologies (Fig. I-6). SufC contains highly conserved sets of amino acid residues including an ABC signature motif, Q-loop, D-loop, and H-motif in addition to the Walker A and Walker B motifs, all of which are characteristic of ABC ATPases (Fig. I-8). I focused on three strictly conserved amino acid residues considered to be essential for ATP hydrolysis in the ABC ATPases (76-78): the Lys residue in the Walker A motif (corresponding to the Lys40 in SufC), the Glu residue immediately following the Walker B motif (the Glu171 in SufC), and the His residue in the H-motif (the His203 in SufC). *In vitro* measurements of ATPase activity clearly demonstrated that SufBCD complexes containing mutated SufC proteins (K40R, E171Q and H203A) almost completely lacked activity (Fig. I-9). These mutations did not impair the structural stability of SufC or its interaction with partner proteins (Fig. I-10). These results prove that as in the canonical ABC ATPase, the residues of the ABC sequence motifs are responsible for ATPase activity in SufC.

To determine whether the ABC ATPase activity of SufC is necessary for the Fe–S cluster biogenesis, I assessed its *in vivo* function using a recently-established method (Takahashi, Y., *submitted for publication*) in the *E. coli Δisc Δsuf* mutant strain UT109 (18). The site-directed mutants of SufC, K40R, E171Q, and H203A, were not able to complement mutant cells, indicating that these residues are indispensable for *in vivo* Fe–S cluster biosynthesis (Fig. I-11). These results are in good agreement with previous experiments regarding the SufC K40R mutant (42). Thus, SufC can behave as an ABC-type ATPase, and the activity is indispensable for *in vivo* Fe–S cluster assembly.

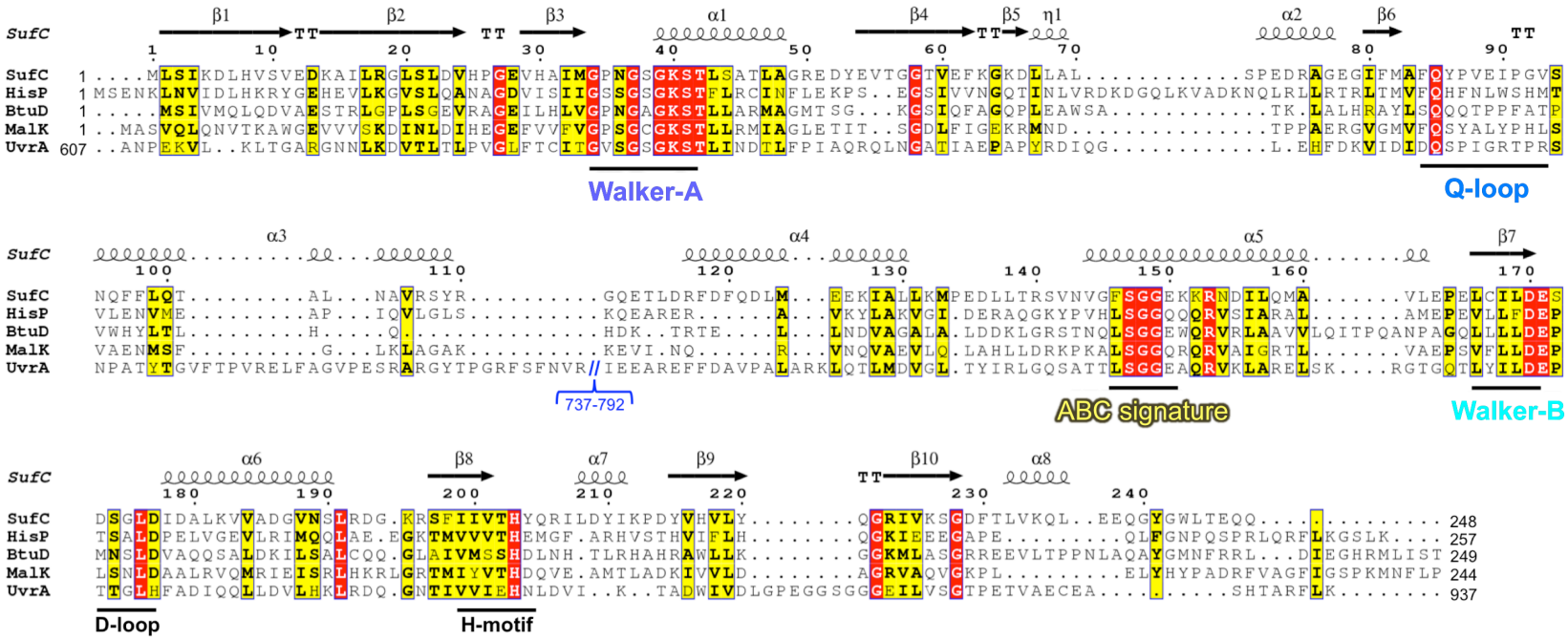

Figure I-8. Sequence alignment of SufC with various ABC ATPases from *E. coli*: HisP, BtuD, MalK, and UvrA. Red and yellow indicate identical and similar residues, respectively. Secondary structures of SufC are shown above the alignment with spirals (α-helices) and arrows (β-strands). Motifs conserved in ABC ATPases are shown below the alignment using the same color-coding scheme as in Fig. I-6. Residues 737-792 in UvrA, an unrelated region, are omitted from the sequence.

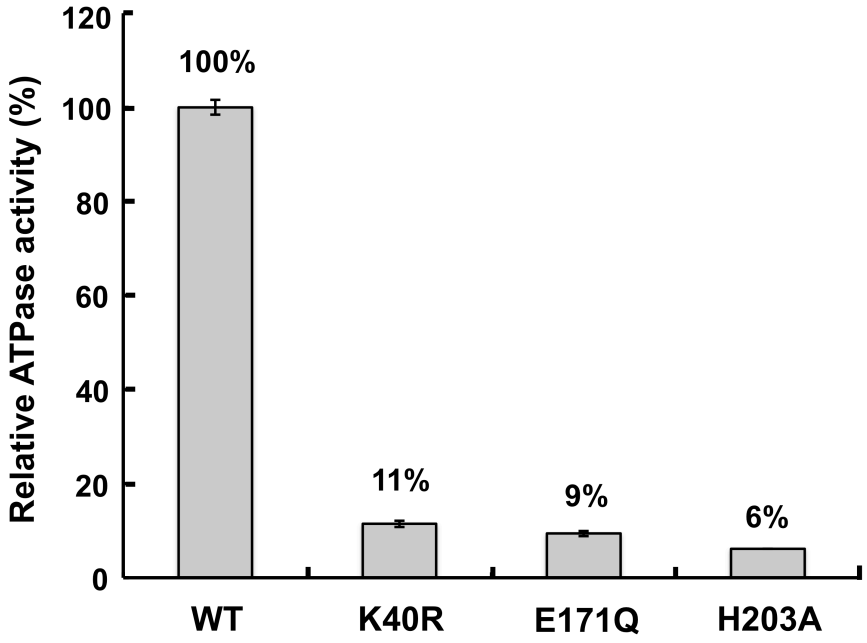

Figure I-9. *In vitro* ATPase activity measurements of the SufBCD complex. Percentages indicate the ratios relative to wild-type complex (~0.07 μmol ATP hydrolyzed min^{-1} mg^{-1}). Error bars, s.d. (n = 3).

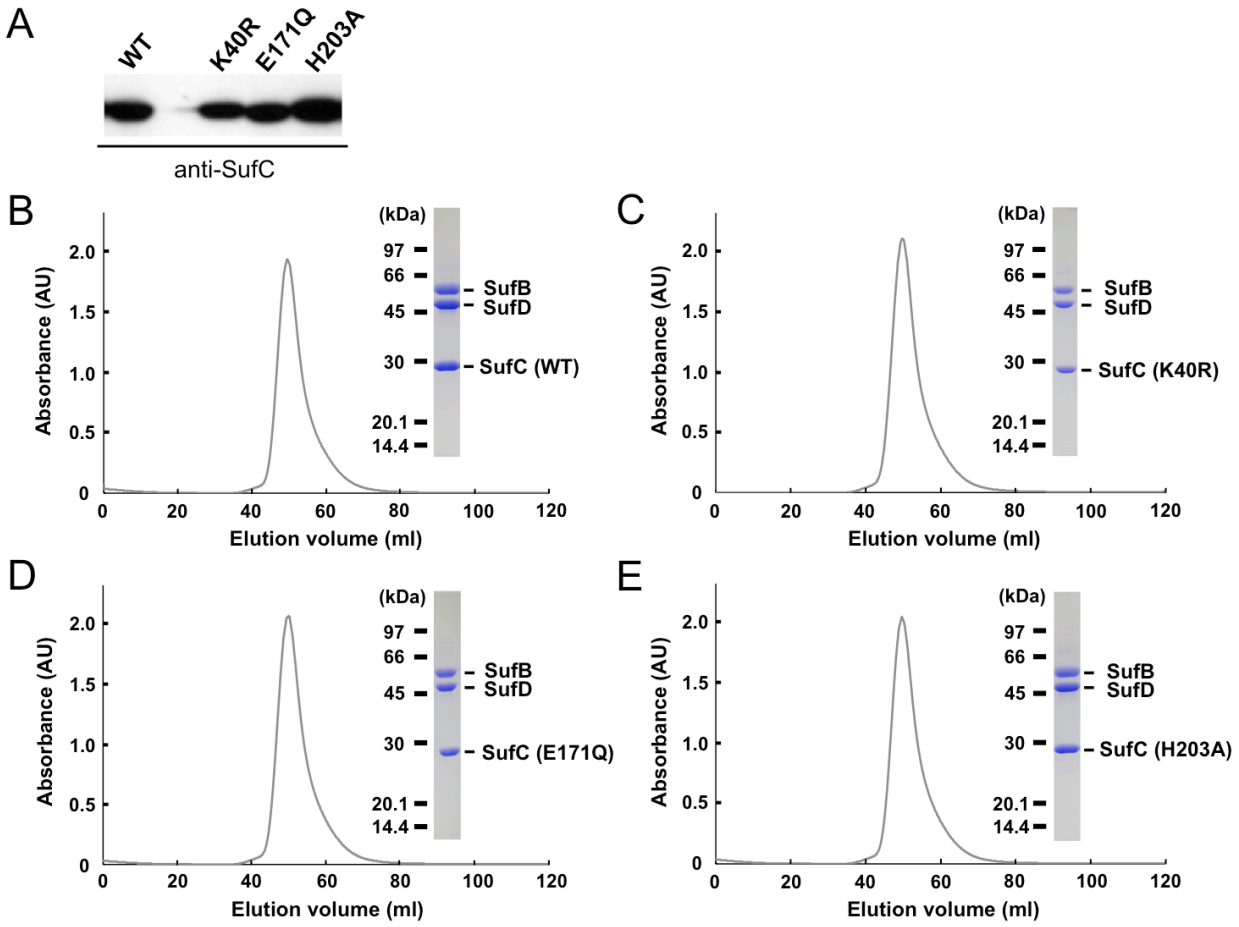

Figure I-10. Mutational analyses of the SufC protein. (A) Comparison of the expression in wild-type and mutant SufC proteins by immunoblot analysis using an antibody against SufC. In the cell, the wild-type and SufC variants are expressed equally. Comparison of the size-exclusion chromatograms of (B) the native SufBCD complex and the SufC mutant complex of (C) K40R, (D) E171Q, and (E) H203A. These SufC mutants form a stable $SufB_1$-$SufC_2$-$SufD_1$ complex similar to the wild-type complex. Elution curves from the gel-filtration column (Sephacryl S-200) are monitored by the absorbance at 280 nm. Inset is SDS-PAGE analysis of each peak fraction.

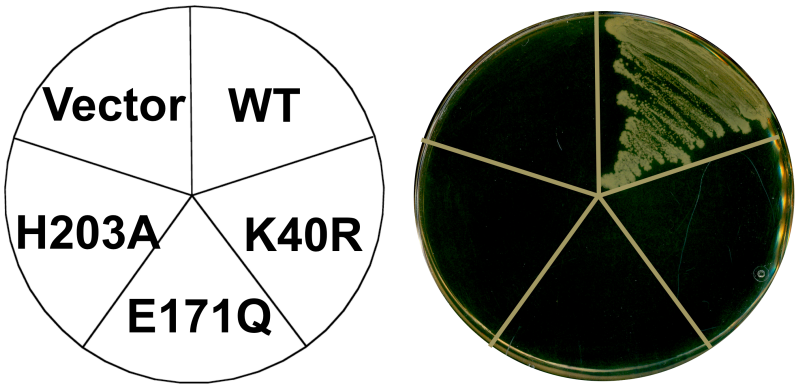

Figure I-11. Phenotypic characterization of the SufC mutations. Growth of the mutant cells (*Δisc Δsuf*) indicates complementation for the loss of *sufC*. Site-directed mutants K40R, E171Q, and H203A of SufC can not complement the *E. coli* UT109 mutant strains, indicating these residues are indispensable for *in vivo* Fe-S cluster biosynthesis.

Discussion

In this study, I determined the crystal structure of the SufBCD complex for the first time, revealing its unusual architecture. The core domains of the SufB–SufD protomers consisted of many long strands (8–13 residues in each strand) arranged in a helical architecture, a so-called β-helix. Indeed, the SufD fold has been categorized as a novel folding superfamily (superhelix turns made of two very long strands each) in the SCOP2 classification database (79). Although the SufB fold has not been classified in any databases yet, the fold was assigned as the same group with SufD by searching the PDBeFold server (80), the 3D alignment program of protein structures with the whole PDB/SCOP archive. Moreover, the respective β-helix core domains in SufB and SufD are associated by anti-parallel β-strands to form a novel heterodimeric structure. In the ABC transporters in general, the transmembrane domains (TMD) consist of a total twelve helices with six helices per monomer, but they have structural diversity appropriate for their respective substrates and functions. In SMC (structural maintenance of chromosome) proteins, family members of ABC proteins, the function-specific domain consists of a long-coiled coil arm that forms a V-shaped dimeric molecule by interacting with the hinge region for DNA binding. Therefore, the novel β-helix architecture of the SufB–SufD protomers appears to be specialized for the Fe–S cluster biogenesis systems.

Despite the structural variations in their substrate- and function-specific domains or subunits, ABC proteins share a common mechanism for transmitting the driving force for their respective functions. Recent extensive structural analyses in ABC transporters revealed that the so-called “transmission interface” transmits the dynamic motion of the ABC ATPase to the TMD during ATP binding and hydrolysis (75), where the Q-loop in the ABC ATPase domain associates with the two short helix-turn-helix motifs in the TMDs. Structural motifs involved in the interaction between SufC and SufB/SufD bear striking similarity to the corresponding configurations in other structurally characterized ABC proteins (Fig. I-12). From a structural

standpoint, the SufBCD complex also shares the mode of the transmission of the driving force with other ABC proteins: the ATPase activity of SufC drives the conformational change of SufB–SufD protomers for Fe–S cluster biogenesis.

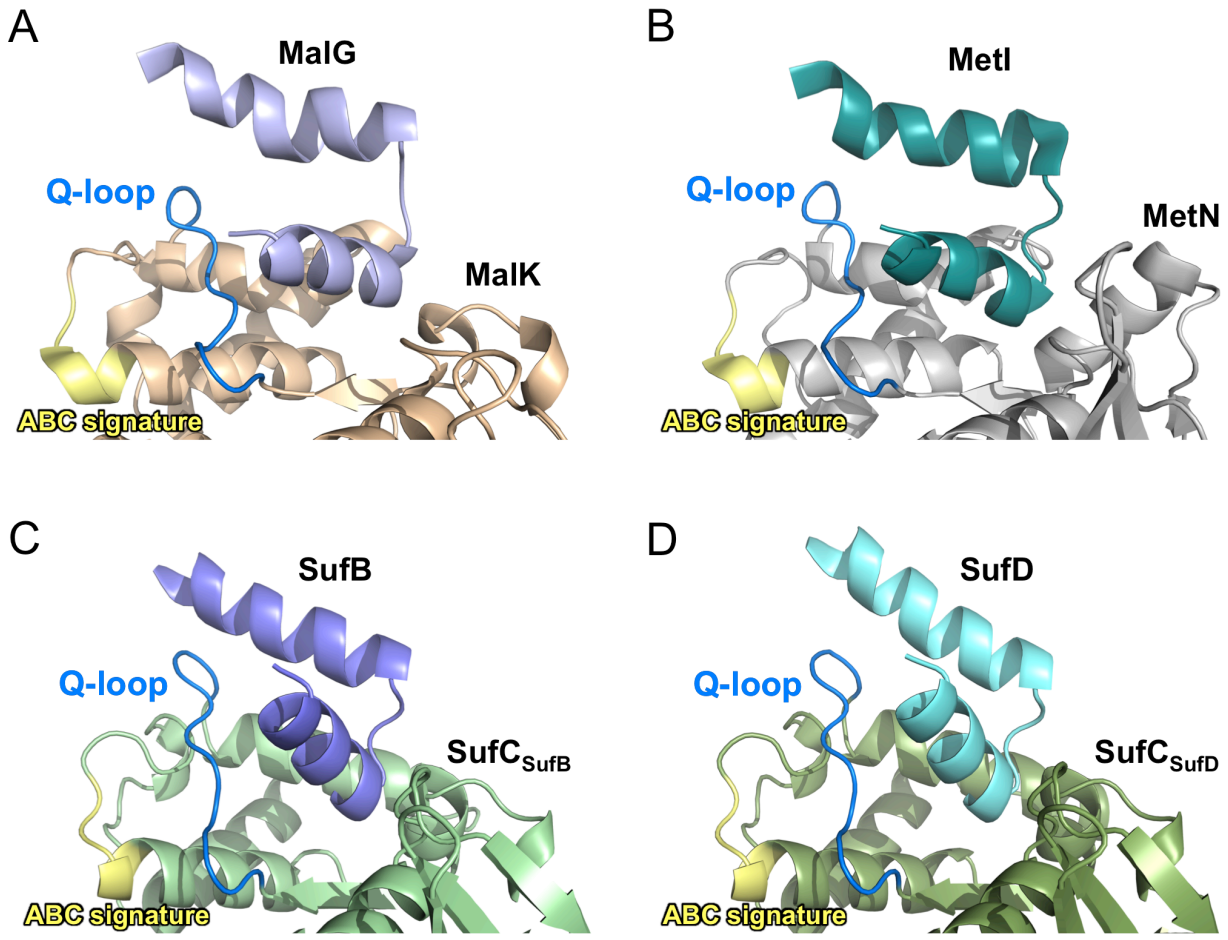

Figure I-12. Comparison of the transmission interface in the SufBCD complex and ABC proteins from *E. coli*. Close-up view of the interface between the substrate/function-specific subunit and the ABC ATPase subunit in (A) the resting (inward-facing) state of MalFGK maltose transporter (PDB code 3FH6), (B) the inward-facing state of the MetNI methionine transporter (PDB code 3DHW), and the resting state of the SufBCD complex at the (C) the SufB-SufC interface, and (D) the SufD-SufC interface. Each subunit in the complex is depicted in a different color. Substrate/function-specific subunit is displayed only for the two short helix-turn-helix involved in the interaction. The orientation and color-coding for the conserved motifs in ABC ATPases are the same as in Fig. I-5.

Chapter II

Functional dynamics revealed by the conformational changes of the SufBCD complex for the *de novo* Fe-S cluster assembly

Abstract

ATP-binding cassette (ABC)-type ATPases are chemo-mechanical engines involved in diverse biological pathways. Recent genomic information reveals that ABC ATPase domains/subunits act not only in ABC transporters and structural maintenance of chromosome (SMC) proteins, but also in iron–sulfur (Fe–S) cluster biogenesis. A novel type of ABC protein, the SufBCD complex, functions in the biosynthesis of nascent Fe–S clusters in almost all Eubacteria and Archaea, as well as eukaryotic chloroplasts. As described in Chapter I, I determined the first crystal structure of the *Escherichia coli* SufBCD complex, which exhibits the common architecture of ABC proteins: two ABC ATPase components (SufC) with function-specific components (SufB–SufD protomers). In this Chapter II, the biochemical and physiological analyses based on this structure provide critical insights into Fe–S cluster assembly and revealed a dynamic conformational change driven by ABC ATPase activity. I propose a molecular mechanism for the biogenesis of the Fe–S cluster in the SufBCD complex.

Introduction

The ATP-binding cassette (ABC) is a ubiquitous, universally conserved ATPase domain/subunit historically defined as the nucleotide-binding domain of an ABC transporter. ABC transporters comprise a large and diverse family of membrane-spanning proteins that transport various substances, ranging from ions to proteins, across membranes (55,81-84). With the availability of complete genomes and the refinement of bioinformatic tools, it has become apparent that ABC-type ATPase domains are present not only in ABC transporters, but also in a variety of non-transporter proteins, the most well-known examples of which are the structural maintenance of chromosome (SMC) proteins involved in chromosome segregation/condensation and DNA repair (85-87). Although the SMC proteins, like the ABC transporters, have attracted great interest because its members are implicated in various human diseases, there are additional types of non-transporter ABC proteins. Here, I focus on a novel type of ABC protein, the SufBCD complex, whose ABC ATPase components (SufC) segregate in a different clade from those of transporters and SMC proteins (Fig. II-1).

The SufBCD complex is a component in the SUF machinery that is responsible for *de novo* iron-sulfur (Fe–S) cluster biogenesis. Although SufC is a member of the ABC ATPase superfamily and exhibits ATPase activity (Chapter I), the role of ATPase activity in Fe–S cluster biogenesis is currently unclear (29,33,34). In ABC transporters, energy from ATP binding/hydrolysis acts to transport specific substances across membranes (55,81-84,88). In soluble SMC proteins, the ABC ATPase utilizes ATP to recognize and bind DNA (55,89). Despite this extreme functional diversity, these proteins share a similar architecture, consisting of two ABC ATPase domains bound to substrate/function-specific partner domains; in both types of proteins, the ABC ATPase activity drives the conformational changes in partner domains required for each function (55). Therefore, it is likely that structural changes in the SufB and SufD subunits are driven by SufC ATPase activity in the SufBCD complex and that the dynamic

motion of the complex should provide important clues regarding the molecular mechanism of Fe–S cluster biogenesis.

In Chapter I, I described the crystal structure of the SufBCD ($SufB_1$-$SufC_2$-$SufD_1$) complex, which exhibits the common configuration of ABC proteins. In this Chapter II, Biochemical experiments based on the crystal structure demonstrated that the two SufC ABC ATPase subunits form a head-to-tail dimer in the complex upon ATP binding, thereby inducing a structural change in the interface between the SufB and SufD subunits. These findings, together with *in vivo* mutational analyses, provided insights into the mechanism of Fe–S cluster assembly in the SufBCD complex.

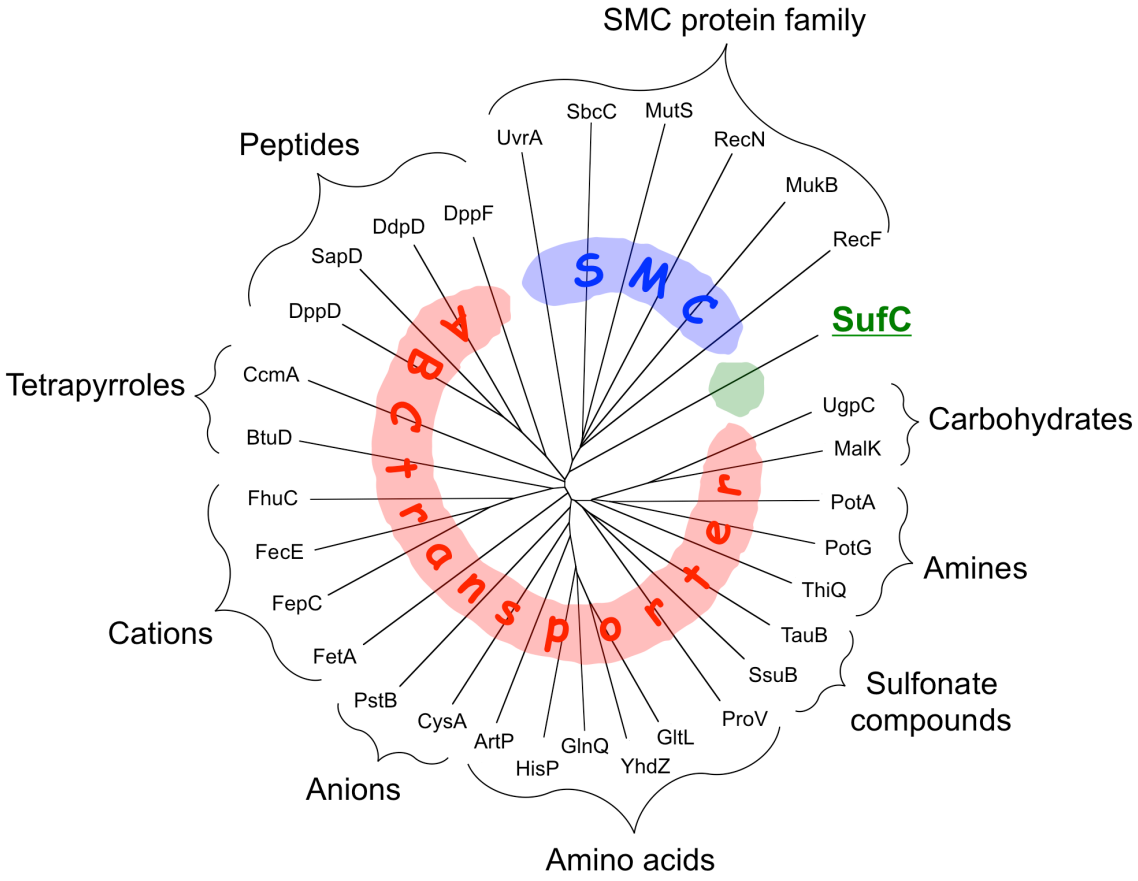

Figure II-1. Dendrogram of ABC ATPases from *E. coli*. Among the 32 proteins, SufC belongs to clades of neither the ABC transporter nor the SMC family.

Experimental procedures

Disulfide cross-linking experiment

The purified mutant complexes (1 mg/ml) were incubated at room temperature for 30 minutes in the presence of 5 mM ATP, 5 mM $MgCl_2$, and 0.05 mM $CuSO_4$, and the resultant products were analyzed by Western blot of native PAGE (7.5% gel) and non-reducing SDS-PAGE (12.5% gel) using antibodies against SufB, SufC, and SufD.

Fluorescence labeling experiment

For assays using 1-anilinonaphthalene-8-sulfonate (ANS), the purified mutant complexes (1 mg/ml) were mixed with 50 μM ATP, 50 μM $MgCl_2$, 5 μM $CuSO_4$, and 30 μM ANS, and time-dependent changes in fluorescence at room temperature was measured for 30 minutes. For the *N*-(7-dimethylamino-4-methylcoumarinyl)-maleimide (DACM) assays, the purified mutant complexes (1 mg/ml) were incubated at room temperature for 30 minutes in the presence of 50 μM ATP, 50 μM $MgCl_2$, 5 μM $CuSO_4$, and 10 μM DACM, and then their fluorescence was measured. All fluorescence spectra were recorded on a FP-8200 fluorescence spectrometer (JASCO).

In vivo Fe–S cluster formation analysis

Site-directed mutagenesis was performed using the pGSO164 plasmid as a template and the primers listed in Table I-1, and the genes were expressed in YT2512 (10). The cells were grown in LB medium containing ampicillin (50 μg/ml) and ferric ammonium citrate (0.1 mg/ml) at 37°C. L-arabinose was added to 0.2% (w/v) final concentration when the cultures obtained an A_{600} of 0.4–0.6. After 3 hours of expression of SufABCDSE at 37°C, the cells were harvested by centrifugation. UV-visible absorption spectra were recorded at room temperature on a V-630 spectrophotometer (JASCO).

Results

Head-to-tail dimer of SufC

The structure of the $SufB_1$–$SufC_2$–$SufD_1$ complex revealed the configuration of each subunit: the SufC subunit of the ABC ATPase binds to the C-terminal helical domains of the SufB/SufD subunits, and the two SufCs are oriented face-to-face (Chapter I). According to the current consensus model, ABC ATPases form a transient head-to-tail dimer in which two nucleotides are sandwiched at the dimer interface between the Walker motifs of one subunit and the ABC signature motif of the other subunit (Fig. II-2A). Based on this concept, I generated a putative dimer model of SufC by superimposing the structure of $SufC_{SufB}$ and $SufC_{SufD}$ onto the dimeric form of the ATP-bound HlyB (H662A) ABC ATPase (77). The resulting model showed that the local structural changes in SufC (mentioned above) enable an ideal association for the head-to-tail dimer without steric hindrances (Fig. II-2B). Despite the favorable modeling results, $SufC_{SufB}$ and $SufC_{SufD}$ subunits are spatially separated in the SufBCD complex, with their ATP-binding motifs facing one another (Fig. I-2B); they would have to move approximately 20 Å closer to each other to form the head-to-tail dimer, a distance that is unusually long compared to other structurally characterized ABC proteins.

I conducted disulfide cross-linking experiments to determine whether the separated SufC subunits could transiently associate with each other in the SufBCD complex. In the putative dimer model, the C_β atoms of Tyr86 in each SufC subunit are in close proximity (< 5.8 Å) (Fig. II-2B). Hence, I replaced Tyr86 with a cysteine to allow for covalent trapping of the transient SufC dimer via disulfide bond formation between the subunits. To simplify analysis, I also replaced the sole native cysteine residue on SufC, Cys167, with an alanine. These mutations did not affect the function of the SufBCD complex (Fig. II-3). After the mutated complex (SufC-Y86C/C167A) was incubated in the presence of ATP/Mg^{2+} and an oxidant ($CuSO_4$) to enhance disulfide-bond formation, disulfide-bond formation was assessed by native PAGE

analysis. The results revealed an additional band on the gel that migrated more quickly than the as-isolated SufBCD complex (Fig. II-2C). No such band was observed when a reducing agent (DTT) was incubated with the sample, indicating that disulfide-bond gives the new band. No additional band was detected when ATP/Mg^{2+} or an oxidant was omitted from the reaction cocktails. Because Western blot analyses using antibodies against SufB, SufC and SufD revealed all of the corresponding signals (Fig. II-2C), I conclude that the novel band represents a conformationally distinct form of the SufBCD complex. In the control experiment using the single-mutated SufBCD complex (SufC-C167A), the corresponding band was undetected. In addition, non-reducing SDS-PAGE/Western blot analyses using an antibody against SufC also revealed an additional band whose molecular size was consistent with a molecule 2-fold larger than SufC (Fig. II-2D). These findings strongly support the idea that SufC can form a transient dimer, even within the SufBCD complex, in the presence of ATP/Mg^{2+}. The mobility shift on native PAGE demonstrates that a structural change occurs in the SufBCD complex upon SufC dimerization.

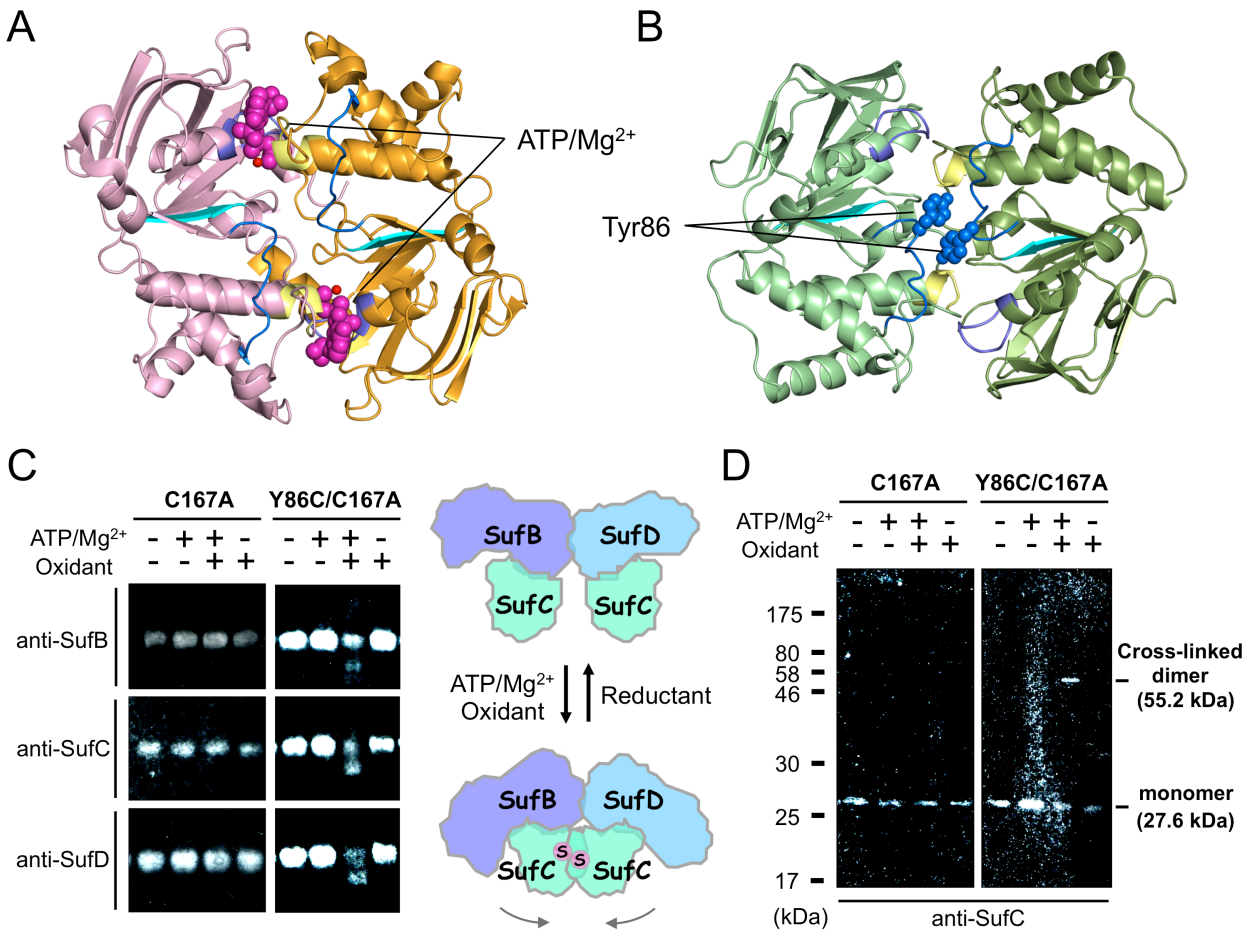

Figure II-2. Disulfide cross-linking analyses of mutated SufBCD complex. (A) Dimeric structure of ABC ATPase HlyB (H662A) (PDB code 1XEF). Light pink and orange indicate individual subunits. Pink and red denote bound ATPs with van der Waals surfaces and Mg^{2+} ions, respectively. Color-coding for the conserved motifs is the same as in Fig. I-6. (B) Putative dimer model of SufC. Docking model is constructed by superimposing $SufC_{SufB}$ and $SufC_{SufD}$ onto the ATP bound HlyB (H662A) dimer. Tyr86 residues are depicted with their van der Waals surfaces. Color-coding for the two subunits and conserved motifs are the same as in Fig. I-2 and Fig. I-6, respectively. (C) Disulfide bond formation between two mutated SufC subunits in the SufBCD complex detected by native PAGE/Western blot analyses using antibodies against SufB, SufC, and SufD. (D) Non-reducing SDS-PAGE/Western blot analyses using an antibody against SufC.

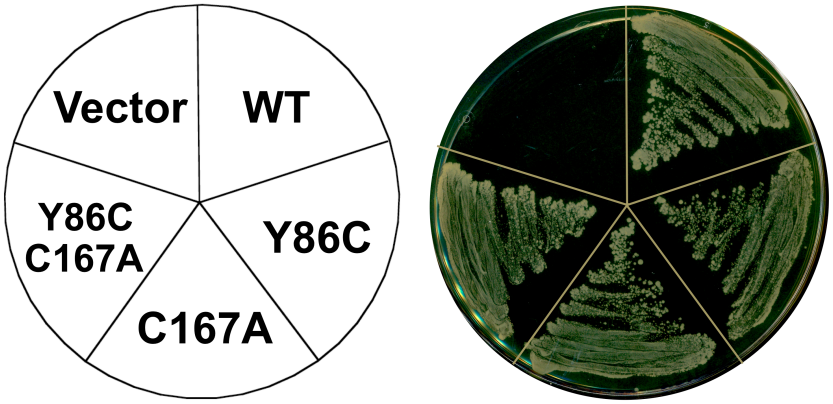

Figure II-3. Phenotypic characterization of the SufC mutations. Growth of the mutant cells (*Δisc Δsuf*) indicates complementation for the loss of *sufC*. Site-directed mutants Y86C, C167A, and Y86C/C167A of SufC can complement the *E. coli* UT109 mutant strain, indicating these mutations do not affect the *in vivo* Fe-S cluster biosynthesis.

Gross structural change of SufB–SufD protomers

I detected the conformational change of the SufBCD complex, initiated by SufC dimerization, in fluorescent labeling experiments using 1-anilinonaphthalene-8-sulfonate (ANS). ANS, which is poorly fluorescent in an aqueous environment, is highly fluorescent upon binding to hydrophobic regions on protein surfaces (90). In order to determine whether SufC dimerization induces the exposure of hydrophobic regions in SufB–SufD protomers, I compared the fluorescence of the native and cross-linked complexes (described above). After adding ATP/Mg^{2+} and an oxidant to the purified mutant SufBCD complex (SufC-Y86C/C167A), I added ANS to the mixture and immediately measured its fluorescence. The results revealed a remarkable increase in fluorescence intensity, depending on the incubation time (Fig. II-4A), indicating that a gross structural change of the SufBCD complex accompanied SufC dimerization (cross-link formation). No such fluorescence increase was observed when ATP/Mg^{2+} or oxidant was omitted from the reaction mixtures, or in a control experiment using the single-mutant SufBCD complex where the dimer is not covalently stabilized (SufC-C167A) (Fig. II-4A). Therefore, this conformational change was surely elicited by SufC dimerization.

Next, I used another fluorescent reagent to determine whether the interface between SufB and SufD protomers is exposed. To this end, I used the fluorescent thiol reagent *N*-(7-dimethylamino-4-methylcoumarinyl)-maleimide (DACM), which has a high quantum yield when it reacts with the free cysteine residues on the protein surface (91). The SufBCD complex has a large number of cysteine residues (13 cysteines in SufB, 3 cysteines in SufD and 1 cysteine in SufC), most of which are buried inside the molecule. I focused on Cys405 of SufB, which is located at the heterodimer interface between the SufB and SufD protomers (Fig. II-5A). This cysteine residue, which is strictly conserved among SufB homologs, is a potential Fe–S cluster assembly site (44). To ascertain whether the Cys405 could be exposed and detected by DACM, I replaced Cys405 of SufB with an alanine, in combination with the SufC-Y86C/C167A mutation.

Each mutant complex (Y86C/C167A/C405A and Y86C/C167A) was incubated under cross-linked conditions (in the presence of ATP/Mg^{2+} and an oxidant) and further incubated after addition of DACM. Fluorescence intensity increased following formation of the SufC cross-linked dimer in the complex, indicating that several cysteine residues in the complex were exposed, whereas a significant decrease in fluorescence intensity was observed upon introduction of the SufB C405A mutation (Fig. II-4B). Control experiments, in which the incubation was performed under non-crosslinked conditions (i.e., in the absence of ATP/Mg^{2+} and oxidant), exhibited no difference between mutant complexes. These results demonstrated that SufC dimer formation leads to exposure of the heterodimer interface of the SufB–SufD protomers (at least of Cys405 of SufB, which is otherwise buried inside the dimer interface). Notably, the invariant residue His360 of SufD, another candidate for the cluster coordination residue (44), is located close to the Cys405 of SufB (Fig. II-5A), strongly implying that His360 of SufD could also be exposed by the conformational change.

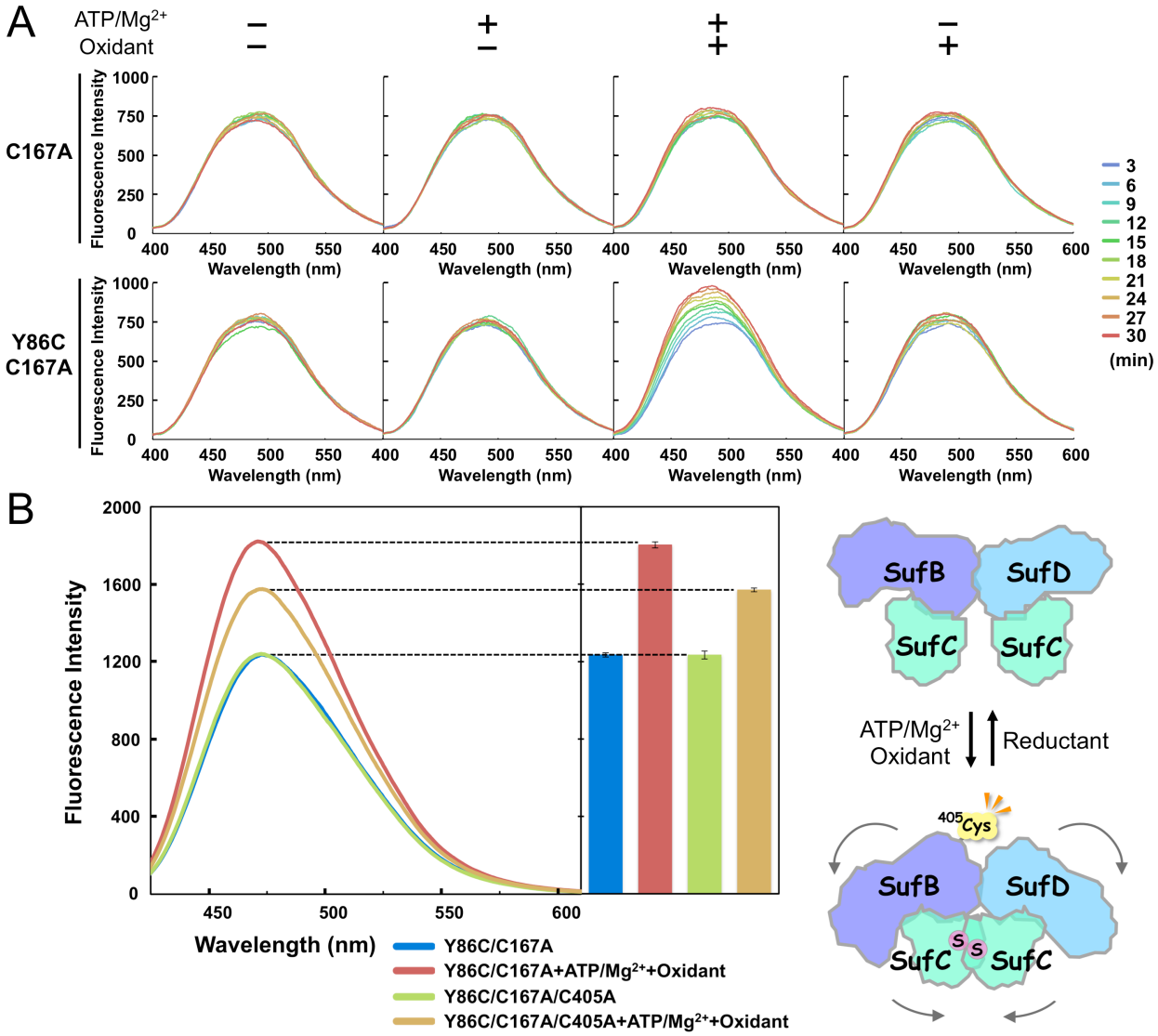

Figure II-4. Fluorescent-labeling analyses of mutated SufBCD complex. (A) ANS detects exposure of hydrophobic regions in SufB-SufD protomers. (B) Exposure of Cys405 of SufB located inside the heterodimer interface between the SufB and SufD protomers under the cross-linked conditions detected by the DACM assays.

In vivo Fe–S cluster formation

During the course of crystallographic phase determination using the heavy atoms, I noticed that two clear electron densities derived from Hg^{2+} ion appeared inside the heterodimer interface between the SufB and SufD protomers (Fig. II-5A): one Hg^{2+} ion bound to Cys405 in SufB, and the other bound to Cys358 in SufD. Hg^{2+}-coordinating cysteine residue from SufB was the invariant Cys405, which is presumably one of the residues composing the assembly site for the nascent Fe–S cluster (44). Interestingly, Cys358 in SufD is located adjacent to His360 of SufD, another candidate for cluster binding. This observation raises the possibility that Hg^{2+} ion binds to the authentic iron-binding site involved in Fe–S cluster assembly. Hence, I performed mutation analyses to ascertain whether these residues function as a cluster assembly site.

Because *in vitro* reconstitution experiments always run the risk that artificial Fe–S clusters will be formed at promiscuous sites (92), I assessed cluster assembly using the color of host cells overproducing the SufBCD complex as well as the SufA, SufS, and SufE components of the pathway. At an early stage of the purification, the fraction containing the SufBCD complex exhibited a blackish-green color; the UV-visible absorption spectrum indicated the presence of a nascent Fe–S cluster with absorption maxima at 340 and 420 nm and a broad shoulder at ~500–650 nm (Fig. II-5B). The color was lost gradually during purification, because the Fe–S cluster is intrinsically fragile with respect to oxygen. Hence, I speculated that cluster formation ability could be evaluated based on the color of the harvested cells prior to exposure of the nascent Fe–S cluster to air by disruption. Harvested cells expressing the wild-type SufBCD complex had a blackish-green color (Fig. II-5C), quite similar to that of the partially purified SufBCD complex (Fig. II-5B, inset). By contrast, control cells harboring only a vector plasmid were an unremarkable white (Fig. II-5C). I thus reasoned that the color of the cells reflects *in vivo* cluster formation ability, at least for the SufBCD complex, even though the cells included other Fe–S proteins.

As expected, both SufB C405A and SufD H360A mutants had white cells, indicating that these residues are indispensable for cluster assembly, whereas Cys358 of SufD, the other binding site for Hg^{2+} ions, was not involved in cluster formation (Fig. II-5C). These results suggest that Cys405 of SufB and His360 of SufD could serve as the *in vivo* cluster binding sites. Furthermore, mutants in residues essential for SufC ATP hydrolysis (K40R, E171Q and H203A; described above) also had white cells (Fig. II-5C). In combination with the findings described above, SufC dimerization and conformational changes are indispensable for nascent Fe–S cluster formation (discussed below). The wild-type and mutant SufBCD proteins were present at equal levels in the cells as confirmed by immunoblot analyses (Fig. II-5D).

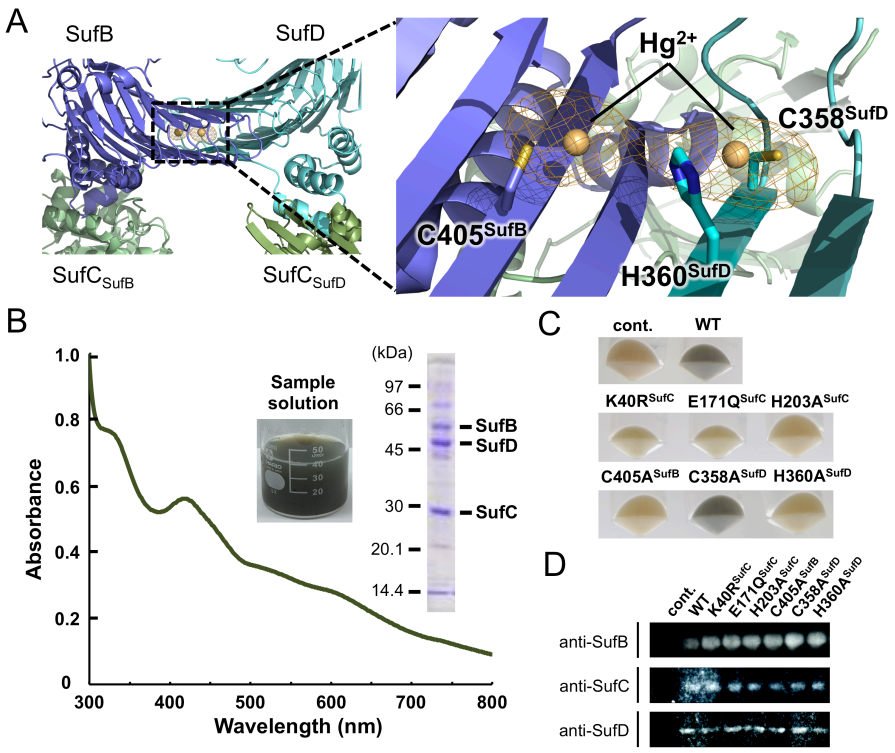

Figure II-5. *In vivo* Fe-S cluster formation on the SufBCD complex. (A) Two strong electron densities derived from the Hg^{2+} ion are observed in the Hg derivative of the SufBCD complex. Anomalous difference map for Hg^{2+} ion is contoured at 6.0 σ. Color-coding scheme for the each subunit is the same as in Fig. I-2. Square denotes the binding site of Hg^{2+}, while right panel shows a close-up view. Two Hg^{2+} ions bound to Cys405 in SufB and Cys358 in SufD are adjacent to His360. These residues are depicted with a stick model, and Hg^{2+} ions are shown as orange balls. (B) UV-visible absorption spectrum of the SufBCD complex at an early purification stage. Inset is the sample solution and SDS-PAGE analysis of the partially purified SufBCD complex used in this measurement. (C) Colors of the harvested host cells overproducing the SufBCD complex and its variants. Blackish green color represents the *in vivo* Fe-S cluster formation on the SufBCD complex. (D) Comparison of the expression level of SuB/SufC/SufD among the cells harboring the wild-type plasmid or the various mutant plasmids by immunoblot analyses using antibodies against SufB, SufC, and SufD.

Discussion

In vitro biochemical experiments and *in vivo* functional analyses based on the crystal structure of the SufBCD complex provided unprecedented insights into the molecular mechanism of Fe–S cluster biogenesis. The main findings are summarized as follows: 1) SufC of ABC-type ATPase forms a transient head-to-tail dimer within the SufBCD complex during the catalytic step of ATP binding and hydrolysis; 2) SufC dimerization drives gross structural changes of the SufB–SufD protomers, leading to the exposure of Cys405 of SufB (and probably also His360 of SufD) inside the heterodimer interface; 3) the conformational changes are directly related to nascent Fe–S cluster formation on the SufBCD complex; 4) Cys405 of SufB and His360 of SufD are most likely to work in concert, possibly serving as the site of *in vivo* cluster synthesis.

Based on these findings, I propose a mechanism for Fe–S cluster biogenesis for the SufBCD complex (Fig. II-6). In the resting state, the SufC ABC-type ATPase in the complex is ready for ATP binding, and the nascent cluster-assembly site at the SufB and SufD interface is buried inside the complex. When SufC forms the head-to-tail dimer upon ATP binding, its dynamic motion is transmitted to the SufB–SufD protomers of the function-specific subunits *via* the transmission interface. Consequently, the invariant residues involved in Fe–S cluster assembly, Cys405 in SufB and His360 in SufD, are exposed to the surface in order to construct and transfer the nascent Fe–S cluster.

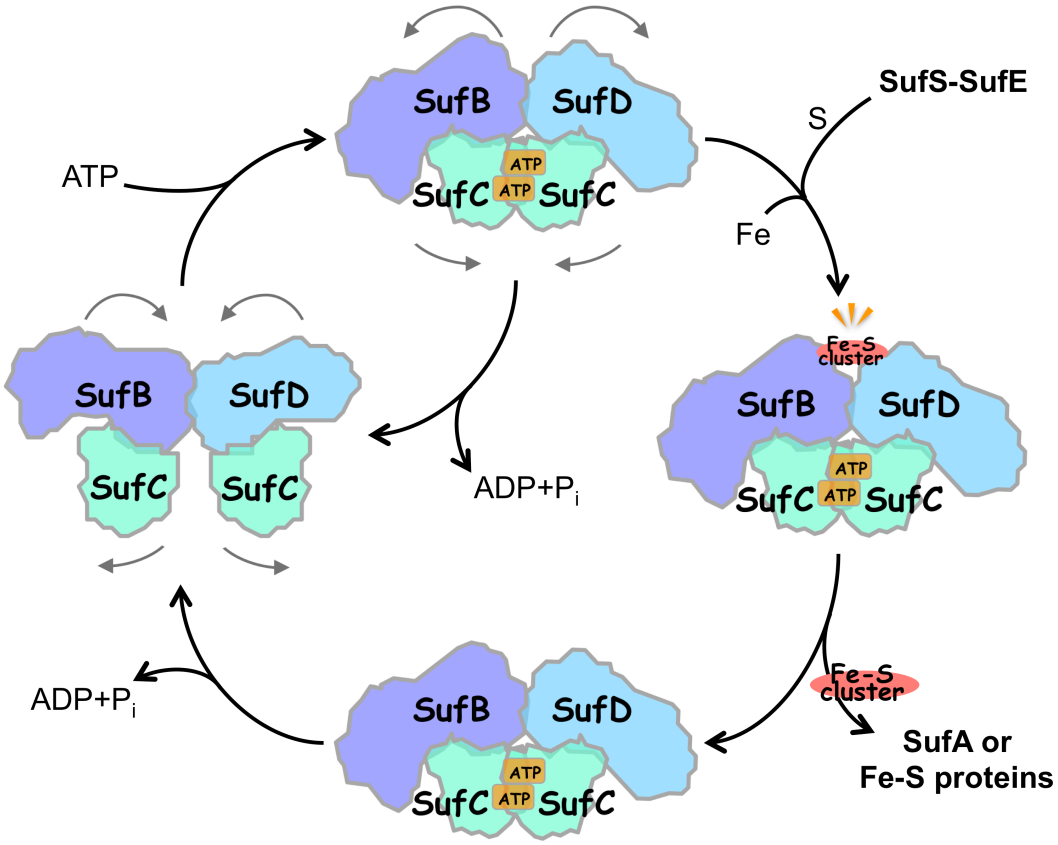

Figure II-6. Proposed mechanism of Fe-S cluster biogenesis for the SufBCD complex. (left) Biogenesis cycle starts in the resting state in which SufC is ready for ATP binding. Upon binding of ATP, SufC forms a head-to-tail dimer. Consequently, the Fe-S cluster binding site between the SufB and SufD interface is exposed to the surface. Nascent Fe-S cluster is built/transferred and ATP is hydrolyzed, restoring the SufBCD complex to its resting state.

General Discussion

Iron-sulfur (Fe-S) proteins that contain an Fe-S cluster as prosthetic group execute a huge spectrum of biochemical tasks including the electron transport (e.g. respiratory complexes and the photosynthetic reaction center) and the regulation of gene expression (2). The versatile characteristics of the Fe-S cluster allow their widespread use in virtually all-living organisms (93). Extensive researches over the past five decades have shed light on the specific/unique function of the Fe-S proteins and their structures (4), but the research for the biosynthetic mechanisms of Fe-S clusters itself were just started from around 2000s (10). The typical Fe-S clusters have the forms of [4Fe-4S], [3Fe-4S] and [2Fe-2S], that is, the clusters have very simple structures (Fig. G-I). Nevertheless, intracellular formation of the Fe–S cluster requires sophisticated system comprising generally a lot of protein components and complexes that mobilize sulfur and iron, assemble nascent clusters, and transfer the assembled clusters to Fe–S proteins (Fig. G-II) (8-10). This system is composed of six proteins encoded by the *sufABCDSE* operon in *E. coli*.

In this thesis, I focused on the SufBCD complex in the SUF system, since this ternary complex could serve as the scaffold for nascent Fe–S cluster assembly (29,33-35). Namely, the structure-function relationship of the SufBCD complex is able to directly elucidate the mechanism of the Fe-S cluster biosynthesis. In this study, the first crystal structure of the *E. coli* SufBCD ($SufB_1$-$SufC_2$–$SufD_1$) complex was determined (Fig. I-1 and I-2), and its structural features were revealed; the complex had the novel β-helix architecture of the SufB–SufD protomers specialized for the Fe–S cluster biosynthesis. Also, my works demonstrated that the ATPase activity of SufC was indispensable for *in vivo* Fe–S cluster assembly (Fig. I-8 – I-11) and utilized to provide the driving force for inducing structural changes of the SufB–SufD protomers (Fig. II-2 – II-4). Furthermore, I identified the assembly site for the nascent Fe–S

cluster inside the heterodimer interface of SufB–SufD protomers, and revealed the correlation between *in vivo* cluster formation and the structural changes (Fig. II-5). Taken together, I proposed, for the first time, the molecular mechanism for the SUF Fe–S cluster biogenesis that incorporates dramatic structural changes driven by the SufC ATPase activity (Fig. II-6).

The SUF Fe–S cluster biogenesis system is phylogenetically diverse and is present in photosynthetic organisms such as higher plants, as well as in Eubacteria and Archaea (10). The SUF machinery is thought to represent the ancestral system for Fe–S cluster biogenesis in all kingdoms of life (18). Genes homologous to SufB and SufC are present in a wide range of bacteria, Archaea, and plastids, suggesting that the SUF system is almost ubiquitous in nature. In this study, I revealed that SufB and SufD share novel structural features. Therefore, the dynamic motion of the $SufB_1$–$SufC_2$–$SufD_1$ complex, experimentally demonstrated here, is universally applicable to all SUF systems, even the $SufB_2$–$SufC_2$ complex in the Archaeal SUF system.

Structural and mechanistic understanding of SUF systems may enable the development of new antibiotics that target the SufBCD complex. Indeed, a recent study demonstrated that the SUF system of malaria parasites is essential for survival and plays a fundamental role in maintaining the apicoplast organelle (94). In eukaryotes, including mammalian cells, the ISC system (95) and its dependent CIA system (96) is responsible for nascent Fe–S cluster biogenesis. The extensively studied scaffold protein of the ISC machinery, IscU, has a completely different sequence and tertiary/quaternary structure than the SufBCD complex (97). Therefore, the SUF system, especially the SufB–SufD protomers with its characteristic β-helix fold and dynamic motion, is an eligible target for drug design with minimal risk of harm to the human body.

References

1. Mortenson, L. E., Valentine, R. C., and Carnahan, J. E. (1962) An electron transport factor from Clostridium pasteurianum. *Biochem Biophys Res Commun* **7**, 448-452
2. Beinert, H., Holm, R. H., and Munck, E. (1997) Iron-sulfur clusters: nature's modular, multipurpose structures. *Science* **277**, 653-659
3. Ruzicka, F. J., and Beinert, H. (1978) The soluble "high potential" type iron-sulfur protein from mitochondria is aconitase. *J Biol Chem* **253**, 2514-2517
4. Johnson, M. K. (1998) Iron-sulfur proteins: new roles for old clusters. *Curr Opin Chem Biol* **2**, 173-181
5. Moulis, J. M., Davasse, V., Golinelli, M.-P., Meyer, J., and Quinkal, I. (1996) The coordination sphere of iron-sulfur clusters: lessons from site-directed mutagenesis experiments. *J Biol Inorg Chem* **1**, 2-14
6. Einsle, O., Tezcan, F. A., Andrade, S. L., Schmid, B., Yoshida, M., Howard, J. B., and Rees, D. C. (2002) Nitrogenase MoFe-protein at 1.16 A resolution: a central ligand in the FeMo-cofactor. *Science* **297**, 1696-1700
7. Malkin, R., and Rabinowitz, J. C. (1966) The reconstitution of clostridial ferredoxin. *Biochem Biophys Res Commun* **23**, 822-827
8. Jacobson, M. R., Cash, V. L., Weiss, M. C., Laird, N. F., Newton, W. E., and Dean, D. R. (1989) Biochemical and genetic analysis of the nifUSVWZM cluster from Azotobacter vinelandii. *Mol Gen Genet* **219**, 49-57
9. Zheng, L., Cash, V. L., Flint, D. H., and Dean, D. R. (1998) Assembly of iron-sulfur clusters. Identification of an iscSUA-hscBA-fdx gene cluster from Azotobacter vinelandii. *J Biol Chem* **273**, 13264-13272
10. Takahashi, Y., and Tokumoto, U. (2002) A third bacterial system for the assembly of

iron-sulfur clusters with homologs in archaea and plastids. *J Biol Chem* **277**, 28380-28383

11. Zheng, L., White, R. H., Cash, V. L., Jack, R. F., and Dean, D. R. (1993) Cysteine desulfurase activity indicates a role for NIFS in metallocluster biosynthesis. *Proc Natl Acad Sci U S A* **90**, 2754-2758
12. Zheng, L., White, R. H., Cash, V. L., and Dean, D. R. (1994) Mechanism for the desulfurization of L-cysteine catalyzed by the nifS gene product. *Biochemistry* **33**, 4714-4720
13. Agar, J. N., Yuvaniyama, P., Jack, R. F., Cash, V. L., Smith, A. D., Dean, D. R., and Johnson, M. K. (2000) Modular organization and identification of a mononuclear iron-binding site within the NifU protein. *J Biol Inorg Chem* **5**, 167-177
14. Yuvaniyama, P., Agar, J. N., Cash, V. L., Johnson, M. K., and Dean, D. R. (2000) NifS-directed assembly of a transient [2Fe-2S] cluster within the NifU protein. *Proc Natl Acad Sci U S A* **97**, 599-604
15. Dos Santos, P. C., Smith, A. D., Frazzon, J., Cash, V. L., Johnson, M. K., and Dean, D. R. (2004) Iron-sulfur cluster assembly: NifU-directed activation of the nitrogenase Fe protein. *J Biol Chem* **279**, 19705-19711
16. Olson, J. W., Agar, J. N., Johnson, M. K., and Maier, R. J. (2000) Characterization of the NifU and NifS Fe-S cluster formation proteins essential for viability in Helicobacter pylori. *Biochemistry* **39**, 16213-16219
17. Ali, V., Shigeta, Y., Tokumoto, U., Takahashi, Y., and Nozaki, T. (2004) An intestinal parasitic protist, Entamoeba histolytica, possesses a non-redundant nitrogen fixation-like system for iron-sulfur cluster assembly under anaerobic conditions. *J Biol Chem* **279**, 16863-16874
18. Tokumoto, U., Kitamura, S., Fukuyama, K., and Takahashi, Y. (2004) Interchangeability

and distinct properties of bacterial Fe-S cluster assembly systems: functional replacement of the *isc* and *suf* operons in *Escherichia coli* with the *nifSU*-like operon from *Helicobacter pylori*. *J Biochem* **136**, 199-209

19. Nakamura, M., Saeki, K., and Takahashi, Y. (1999) Hyperproduction of recombinant ferredoxins in *Escherichia coli* by coexpression of the ORF1-ORF2-*iscS*-*iscU*-*iscA*-*hscB*-*hscA*-*fdx*-ORF3 gene cluster. *J Biochem* **126**, 10-18
20. Tokumoto, U., and Takahashi, Y. (2001) Genetic analysis of the isc operon in *Escherichia coli* involved in the biogenesis of cellular iron-sulfur proteins. *J Biochem* **130**, 63-71
21. Ollagnier-de-Choudens, S., Mattioli, T., Takahashi, Y., and Fontecave, M. (2001) Iron-sulfur cluster assembly: characterization of IscA and evidence for a specific and functional complex with ferredoxin. *J Biol Chem* **276**, 22604-22607
22. Krebs, C., Agar, J. N., Smith, A. D., Frazzon, J., Dean, D. R., Huynh, B. H., and Johnson, M. K. (2001) IscA, an alternate scaffold for Fe-S cluster biosynthesis. *Biochemistry* **40**, 14069-14080
23. Ding, H., Clark, R. J., and Ding, B. (2004) IscA mediates iron delivery for assembly of iron-sulfur clusters in IscU under the limited accessible free iron conditions. *J Biol Chem* **279**, 37499-37504
24. Ding, H., Harrison, K., and Lu, J. (2005) Thioredoxin reductase system mediates iron binding in IscA and iron delivery for the iron-sulfur cluster assembly in IscU. *J Biol Chem* **280**, 30432-30437
25. Schwartz, C. J., Giel, J. L., Patschkowski, T., Luther, C., Ruzicka, F. J., Beinert, H., and Kiley, P. J. (2001) IscR, an Fe-S cluster-containing transcription factor, represses expression of *Escherichia coli* genes encoding Fe-S cluster assembly proteins. *Proc Natl Acad Sci U S A* **98**, 14895-14900

26. Lee, J. H., Yeo, W. S., and Roe, J. H. (2004) Induction of the sufA operon encoding Fe-S assembly proteins by superoxide generators and hydrogen peroxide: involvement of OxyR, IHF and an unidentified oxidant-responsive factor. *Mol Microbiol* **51**, 1745-1755

27. Outten, F. W., Djaman, O., and Storz, G. (2004) A *suf* operon requirement for Fe-S cluster assembly during iron starvation in *Escherichia coli*. *Mol Microbiol* **52**, 861-872

28. Loiseau, L., Ollagnier-de-Choudens, S., Nachin, L., Fontecave, M., and Barras, F. (2003) Biogenesis of Fe-S cluster by the bacterial Suf system: SufS and SufE form a new type of cysteine desulfurase. *J Biol Chem* **278**, 38352-38359

29. Outten, F. W., Wood, M. J., Munoz, F. M., and Storz, G. (2003) The SufE protein and the SufBCD complex enhance SufS cysteine desulfurase activity as part of a sulfur transfer pathway for Fe-S cluster assembly in *Escherichia coli*. *J Biol Chem* **278**, 45713-45719

30. Ollagnier-de Choudens, S., Nachin, L., Sanakis, Y., Loiseau, L., Barras, F., and Fontecave, M. (2003) SufA from Erwinia chrysanthemi. Characterization of a scaffold protein required for iron-sulfur cluster assembly. *J Biol Chem* **278**, 17993-18001

31. Lu, J., Yang, J., Tan, G., and Ding, H. (2008) Complementary roles of SufA and IscA in the biogenesis of iron-sulfur clusters in *Escherichia coli*. *Biochem J* **409**, 535-543

32. Gupta, V., Sendra, M., Naik, S. G., Chahal, H. K., Huynh, B. H., Outten, F. W., Fontecave, M., and Ollagnier de Choudens, S. (2009) Native *Escherichia coli* SufA, coexpressed with SufBCDSE, purifies as a [2Fe-2S] protein and acts as an Fe-S transporter to Fe-S target enzymes. *J Am Chem Soc* **131**, 6149-6153

33. Nachin, L., Loiseau, L., Expert, D., and Barras, F. (2003) SufC: an unorthodox cytoplasmic ABC/ATPase required for [Fe-S] biogenesis under oxidative stress. *EMBO J* **22**, 427-437

34. Chahal, H. K., Dai, Y., Saini, A., Ayala-Castro, C., and Outten, F. W. (2009) The SufBCD Fe-S scaffold complex interacts with SufA for Fe-S cluster transfer.

Biochemistry **48**, 10644-10653

35. Wollers, S., Layer, G., Garcia-Serres, R., Signor, L., Clemancey, M., Latour, J. M., Fontecave, M., and Ollagnier de Choudens, S. (2010) Iron-sulfur (Fe-S) cluster assembly: the SufBCD complex is a new type of Fe-S scaffold with a flavin redox cofactor. *J Biol Chem* **285**, 23331-23341
36. Boyd, E. S., Thomas, K. M., Dai, Y., Boyd, J. M., and Outten, F. W. (2014) Interplay between oxygen and Fe-S cluster biogenesis: insights from the Suf pathway. *Biochemistry* **53**, 5834-5847
37. Mihara, H., Maeda, M., Fujii, T., Kurihara, T., Hata, Y., and Esaki, N. (1999) A nifS-like gene, csdB, encodes an *Escherichia coli* counterpart of mammalian selenocysteine lyase. Gene cloning, purification, characterization and preliminary x-ray crystallographic studies. *J Biol Chem* **274**, 14768-14772
38. Ollagnier-de-Choudens, S., Lascoux, D., Loiseau, L., Barras, F., Forest, E., and Fontecave, M. (2003) Mechanistic studies of the SufS-SufE cysteine desulfurase: evidence for sulfur transfer from SufS to SufE. *FEBS Lett* **555**, 263-267
39. Vinella, D., Brochier-Armanet, C., Loiseau, L., Talla, E., and Barras, F. (2009) Iron-sulfur (Fe/S) protein biogenesis: phylogenomic and genetic studies of A-type carriers. *PLoS Genet* **5**, e1000497
40. Rangachari, K., Davis, C. T., Eccleston, J. F., Hirst, E. M., Saldanha, J. W., Strath, M., and Wilson, R. J. (2002) SufC hydrolyzes ATP and interacts with SufB from *Thermotoga maritima*. *FEBS Lett* **514**, 225-228
41. Kitaoka, S., Wada, K., Hasegawa, Y., Minami, Y., Fukuyama, K., and Takahashi, Y. (2006) Crystal structure of *Escherichia coli* SufC, an ABC-type ATPase component of the SUF iron-sulfur cluster assembly machinery. *FEBS Lett* **580**, 137-143
42. Saini, A., Mapolelo, D. T., Chahal, H. K., Johnson, M. K., and Outten, F. W. (2010)

SufD and SufC ATPase activity are required for iron acquisition during in vivo Fe-S cluster formation on SufB. *Biochemistry* **49**, 9402-9412

43. Petrovic, A., Davis, C. T., Rangachari, K., Clough, B., Wilson, R. J., and Eccleston, J. F. (2008) Hydrodynamic characterization of the SufBC and SufCD complexes and their interaction with fluorescent adenosine nucleotides. *Protein Sci* **17**, 1264-1274

44. Wada, K., Sumi, N., Nagai, R., Iwasaki, K., Sato, T., Suzuki, K., Hasegawa, Y., Kitaoka, S., Minami, Y., Outten, F. W., Takahashi, Y., and Fukuyama, K. (2009) Molecular dynamism of Fe-S cluster biosynthesis implicated by the structure of the $SufC_2$-$SufD_2$ complex. *J Mol Biol* **387**, 245-258

45. Eccleston, J. F., Petrovic, A., Davis, C. T., Rangachari, K., and Wilson, R. J. (2006) The kinetic mechanism of the SufC ATPase: the cleavage step is accelerated by SufB. *J Biol Chem* **281**, 8371-8378

46. Layer, G., Gaddam, S. A., Ayala-Castro, C. N., Ollagnier-de Choudens, S., Lascoux, D., Fontecave, M., and Outten, F. W. (2007) SufE transfers sulfur from SufS to SufB for iron-sulfur cluster assembly. *J Biol Chem* **282**, 13342-13350

47. Mihara, H., Fujii, T., Kato, S., Kurihara, T., Hata, Y., and Esaki, N. (2002) Structure of external aldimine of *Escherichia coli* CsdB, an IscS/NifS homolog: implications for its specificity toward selenocysteine. *J Biochem* **131**, 679-685

48. Goldsmith-Fischman, S., Kuzin, A., Edstrom, W. C., Benach, J., Shastry, R., Xiao, R., Acton, T. B., Honig, B., Montelione, G. T., and Hunt, J. F. (2004) The SufE sulfur-acceptor protein contains a conserved core structure that mediates interdomain interactions in a variety of redox protein complexes. *J Mol Biol* **344**, 549-565

49. Wada, K., Hasegawa, Y., Gong, Z., Minami, Y., Fukuyama, K., and Takahashi, Y. (2005) Crystal structure of *Escherichia coli* SufA involved in biosynthesis of iron-sulfur clusters: implications for a functional dimer. *FEBS Lett* **579**, 6543-6548

50. Badger, J., Sauder, J. M., Adams, J. M., Antonysamy, S., Bain, K., Bergseid, M. G., Buchanan, S. G., Buchanan, M. D., Batiyenko, Y., Christopher, J. A., Emtage, S., Eroshkina, A., Feil, I., Furlong, E. B., Gajiwala, K. S., Gao, X., He, D., Hendle, J., Huber, A., Hoda, K., Kearins, P., Kissinger, C., Laubert, B., Lewis, H. A., Lin, J., Loomis, K., Lorimer, D., Louie, G., Maletic, M., Marsh, C. D., Miller, I., Molinari, J., Muller-Dieckmann, H. J., Newman, J. M., Noland, B. W., Pagarigan, B., Park, F., Peat, T. S., Post, K. W., Radojicic, S., Ramos, A., Romero, R., Rutter, M. E., Sanderson, W. E., Schwinn, K. D., Tresser, J., Winhoven, J., Wright, T. A., Wu, L., Xu, J., and Harris, T. J. (2005) Structural analysis of a set of proteins resulting from a bacterial genomics project. *Proteins* **60**, 787-796

51. Fujii, T., Maeda, M., Mihara, H., Kurihara, T., Esaki, N., and Hata, Y. (2000) Structure of a NifS homologue: X-ray structure analysis of CsdB, an *Escherichia coli* counterpart of mammalian selenocysteine lyase. *Biochemistry* **39**, 1263-1273

52. Cupp-Vickery, J. R., Urbina, H., and Vickery, L. E. (2003) Crystal structure of IscS, a cysteine desulfurase from *Escherichia coli*. *J Mol Biol* **330**, 1049-1059

53. Mihara, H., Kurihara, T., Yoshimura, T., and Esaki, N. (2000) Kinetic and mutational studies of three NifS homologs from *Escherichia coli*: mechanistic difference between L-cysteine desulfurase and L-selenocysteine lyase reactions. *J Biochem* **127**, 559-567

54. Watanabe, S., Kita, A., and Miki, K. (2005) Crystal structure of atypical cytoplasmic ABC-ATPase SufC from Thermus thermophilus HB8. *J Mol Biol* **353**, 1043-1054

55. Hopfner, K. P., and Tainer, J. A. (2003) Rad50/SMC proteins and ABC transporters: unifying concepts from high-resolution structures. *Curr Opin Struct Biol* **13**, 249-255

56. Otwinowski, Z., and Minor, W. (1997) Processing of X-ray diffraction data collected in oscillation mode. in *Methods in Enzymology* (Charles W. Carter, Jr. ed.), Academic Press. pp 307-326

57. Adams, P. D., Afonine, P. V., Bunkoczi, G., Chen, V. B., Davis, I. W., Echols, N., Headd, J. J., Hung, L. W., Kapral, G. J., Grosse-Kunstleve, R. W., McCoy, A. J., Moriarty, N. W., Oeffner, R., Read, R. J., Richardson, D. C., Richardson, J. S., Terwilliger, T. C., and Zwart, P. H. (2010) *PHENIX*: a comprehensive Python-based system for macromolecular structure solution. *Acta Crystallogr D Biol Crystallogr* **66**, 213-221

58. Emsley, P., Lohkamp, B., Scott, W. G., and Cowtan, K. (2010) Features and development of *Coot*. *Acta Crystallogr D Biol Crystallogr* **66**, 486-501

59. Hutchinson, E. G., and Thornton, J. M. (1996) PROMOTIF--a program to identify and analyze structural motifs in proteins. *Protein Sci* **5**, 212-220

60. Laskowski, R. A., MacArthur, M. W., Moss, D. S., and Thornton, J. M. (1993) *PROCHECK*: a program to check the stereochemical quality of protein structures. *Journal of Applied Crystallography* **26**, 283-291

61. Kleywegt, G. (1996) Use of non-crystallographic symmetry in protein structure refinement. *Acta Crystallographica Section D* **52**, 842-857

62. Schrödinger, L. (2010) The PyMOL Molecular Graphics System, Version 1.3r1.

63. Pettersen, E. F., Goddard, T. D., Huang, C. C., Couch, G. S., Greenblatt, D. M., Meng, E. C., and Ferrin, T. E. (2004) UCSF Chimera--a visualization system for exploratory research and analysis. *J Comput Chem* **25**, 1605-1612

64. Shaikh, T. R., Gao, H., Baxter, W. T., Asturias, F. J., Boisset, N., Leith, A., and Frank, J. (2008) SPIDER image processing for single-particle reconstruction of biological macromolecules from electron micrographs. *Nat Protoc* **3**, 1941-1974

65. Ludtke, S. J., Baldwin, P. R., and Chiu, W. (1999) EMAN: semiautomated software for high-resolution single-particle reconstructions. *J Struct Biol* **128**, 82-97

66. Petoukhov, M. V., Franke, D., Shkumatov, A. V., Tria, G., Kikhney, A. G., Gajda, M., Gorba, C., Mertens, H. D., Konarev, P. V., and Svergun, D. I. (2012) New developments

in the *ATSAS* program package for small-angle scattering data analysis. *J Appl Crystallogr* **45**, 342-350

67. Svergun, D., Barberato, C., and Koch, M. H. J. (1995) *CRYSOL* - a program to evaluate X-ray solution scattering of biological macromolecules from atomic coordinates. *Journal of Applied Crystallography* **28**, 768-773

68. Franke, D., and Svergun, D. I. (2009) *DAMMIF*, a program for rapid ab-initio shape determination in small-angle scattering. *Journal of Applied Crystallography* **42**, 342-346

69. Volkov, V. V., and Svergun, D. I. (2003) Uniqueness of *ab initio* shape determination in small-angle scattering. *Journal of Applied Crystallography* **36**, 860-864

70. Kovach, M. E., Elzer, P. H., Hill, D. S., Robertson, G. T., Farris, M. A., Roop, R. M., 2nd, and Peterson, K. M. (1995) Four new derivatives of the broad-host-range cloning vector pBBR1MCS, carrying different antibiotic-resistance cassettes. *Gene* **166**, 175-176

71. Sievers, F., Wilm, A., Dineen, D., Gibson, T. J., Karplus, K., Li, W., Lopez, R., McWilliam, H., Remmert, M., Soding, J., Thompson, J. D., and Higgins, D. G. (2011) Fast, scalable generation of high-quality protein multiple sequence alignments using Clustal Omega. *Mol Syst Biol* **7**, 539

72. Perriere, G., and Gouy, M. (1996) WWW-query: an on-line retrieval system for biological sequence banks. *Biochimie* **78**, 364-369

73. Robert, X., and Gouet, P. (2014) Deciphering key features in protein structures with the new ENDscript server. *Nucleic Acids Res* **42**, W320-324

74. Zhou, J., and Rudd, K. E. (2013) EcoGene 3.0. *Nucleic Acids Res* **41**, D613-624

75. Hollenstein, K., Dawson, R. J., and Locher, K. P. (2007) Structure and mechanism of ABC transporter proteins. *Curr Opin Struct Biol* **17**, 412-418

76. Smith, P. C., Karpowich, N., Millen, L., Moody, J. E., Rosen, J., Thomas, P. J., and Hunt, J. F. (2002) ATP binding to the motor domain from an ABC transporter drives formation

of a nucleotide sandwich dimer. *Mol Cell* **10**, 139-149

77. Zaitseva, J., Jenewein, S., Jumpertz, T., Holland, I. B., and Schmitt, L. (2005) H662 is the linchpin of ATP hydrolysis in the nucleotide-binding domain of the ABC transporter HlyB. *EMBO J* **24**, 1901-1910

78. Hung, L. W., Wang, I. X., Nikaido, K., Liu, P. Q., Ames, G. F., and Kim, S. H. (1998) Crystal structure of the ATP-binding subunit of an ABC transporter. *Nature* **396**, 703-707

79. Andreeva, A., Howorth, D., Chothia, C., Kulesha, E., and Murzin, A. G. (2014) SCOP2 prototype: a new approach to protein structure mining. *Nucleic Acids Res* **42**, D310-314

80. Krissinel, E., and Henrick, K. (2004) Secondary-structure matching (SSM), a new tool for fast protein structure alignment in three dimensions. *Acta Crystallogr D Biol Crystallogr* **60**, 2256-2268

81. Higgins, C. F. (1992) ABC transporters: from microorganisms to man. *Annu Rev Cell Biol* **8**, 67-113

82. Schmitt, L., and Tampe, R. (2002) Structure and mechanism of ABC transporters. *Curr Opin Struct Biol* **12**, 754-760

83. Locher, K. P., Lee, A. T., and Rees, D. C. (2002) The *E. coli* BtuCD structure: a framework for ABC transporter architecture and mechanism. *Science* **296**, 1091-1098

84. Holland, I. B., and Blight, M. A. (1999) ABC-ATPases, adaptable energy generators fuelling transmembrane movement of a variety of molecules in organisms from bacteria to humans. *J Mol Biol* **293**, 381-399

85. Hirano, T. (2005) SMC proteins and chromosome mechanics: from bacteria to humans. *Philos Trans R Soc Lond B Biol Sci* **360**, 507-514

86. Hopfner, K. P., Karcher, A., Shin, D. S., Craig, L., Arthur, L. M., Carney, J. P., and Tainer, J. A. (2000) Structural biology of Rad50 ATPase: ATP-driven conformational control in DNA double-strand break repair and the ABC-ATPase superfamily. *Cell* **101**,

789-800

87. Graumann, P. L. (2001) SMC proteins in bacteria: condensation motors for chromosome segregation? *Biochimie* **83**, 53-59

88. Hyde, S. C., Emsley, P., Hartshorn, M. J., Mimmack, M. M., Gileadi, U., Pearce, S. R., Gallagher, M. P., Gill, D. R., Hubbard, R. E., and Higgins, C. F. (1990) Structural model of ATP-binding proteins associated with cystic fibrosis, multidrug resistance and bacterial transport. *Nature* **346**, 362-365

89. Hirano, T. (2002) The ABCs of SMC proteins: two-armed ATPases for chromosome condensation, cohesion, and repair. *Genes Dev* **16**, 399-414

90. Hawe, A., Sutter, M., and Jiskoot, W. (2008) Extrinsic fluorescent dyes as tools for protein characterization. *Pharm Res* **25**, 1487-1499

91. Namihisa, T., Saifuku, K., Ishii, H., Watanabe, S., and Sekine, T. (1983) *N*-(7-dimethylamino-4-methylcoumarinyl)-maleimide (DACM): an alternative label for fluorescence tracing. *J Immunol Methods* **56**, 125-134

92. Arakawa, S., and Kimura, T. (1979) Preparation and partial characterization of iron-sulfur, iron-selenium, and iron-tellurium complexes of bovine serum albumin. *Biochim Biophys Acta* **580**, 382-391

93. Rees, D. C., and Howard, J. B. (2003) The interface between the biological and inorganic worlds: iron-sulfur metalloclusters. *Science* **300**, 929-931

94. Gisselberg, J. E., Dellibovi-Ragheb, T. A., Matthews, K. A., Bosch, G., and Prigge, S. T. (2013) The suf iron-sulfur cluster synthesis pathway is required for apicoplast maintenance in malaria parasites. *PLoS Pathog* **9**, e1003655

95. Johnson, D. C., Dean, D. R., Smith, A. D., and Johnson, M. K. (2005) Structure, function, and formation of biological iron-sulfur clusters. *Annu Rev Biochem* **74**, 247-281

96. Lill, R. (2009) Function and biogenesis of iron-sulphur proteins. *Nature* **460**, 831-838

97. Shimomura, Y., Wada, K., Fukuyama, K., and Takahashi, Y. (2008) The asymmetric trimeric architecture of [2Fe-2S] IscU: implications for its scaffolding during iron-sulfur cluster biosynthesis. *J Mol Biol* **383**, 133-143

List of Publications

Paper related to this thesis

Hirabayashi K., Yuda E., Tanaka N., Katayama S., Iwasaki K., Matsumoto T., Kurisu G., Outten F. W., Fukuyama K., Takahashi Y., and Wada K. (2015) Functional Dynamics Revealed by the Structure of the SufBCD Complex, a Novel ATP-binding Cassette (ABC) Protein That Serves as a Scaffold for Iron-Sulfur Cluster Biogenesis. *J Biol Chem*, in press.

Other papers

Kameda H., Hirabayashi K., Wada K., and Fukuyama K. (2011) Mapping of Protein-Protein Interaction Sites in the Plant-Type [2Fe-2S] Ferredoxin. *PLoS ONE* **6**, e21947

Kamachi S., Hirabayashi K., Tamoi M., Shigeoka S., Tada T., and Wada K. (2015) The crystal structure of isoniazid-bound KatG catalase-peroxidase from *Synechococcus elongatus* PCC7942. *FEBS Journal* **282**, 54-64

Kamachi S., Hirabayashi K., Tamoi M., Shigeoka S., Tada T., and Wada K. (2015) Crystal structure of the catalase-peroxidase KatG W78F mutant from *Synechococcus elongatus* PCC7942 in complex with the antitubercular pro-drug isoniazid. *FEBS Letters* **589**, 131-137

Acknowledgements

This work has been carried out under the direction of Assoc. Prof. K. Wada (University of Miyazaki) and Prof. G. Kurisu (Osaka University). I am sincerely grateful to Assoc. Prof. Wada for his supports, encouragement, fruitful discussions, and guidance throughout this study. I am grateful to Prof. Kurisu, Prof. K. Fukuyama (Osaka University), Prof. Y. Takahashi (Saitama University), Prof. T. Hase, Prof. A. Nakagawa, and Assoc. Prof. M. Nakai (Osaka University) for their encouragement, helpful advises and discussions. I also greatly thank to Dr. S. Katayama, and Assoc. Prof. K. Iwasaki (Osaka University) for their aid with single-particle EM reconstructions, Dr. T. Matsumoto (Rigaku Corporation) for his aid with SAXS experiments, Mr. E. Yuda, Mr. N. Tanaka, and Ms. Y. Erikawa (Saitama University) for their help with plasmid construction and complementation experiments, Prof. F. W. Outten (University of South Carolina) for kindly providing the plasmid, Dr. E. Yamashita, Dr. A. Higashiura (Osaka University), Dr. K. Hirata, Dr. K. Yamashita (RIKEN), and Assoc. Prof. M. Sugishima (Kurume University) for their assistance with data collection at the SPring-8 synchrotron radiation facility, Mr. H. Omori (Osaka University) for technical assistance for nucleotide sequencing, Dr. T. Ishizuka, and Prof. Y. Xu (University of Miyazaki) for their assistance with fluorescence measurements,. Finally, I thank all members of Wada laboratory and Kurisu laboratory for their tremendous supports and valuable discussions.